Supporting Information

Specific Esterase and pH Logically Regulate ESIPT: Different Kinds of Granulocytes Sorting

Kui Wang,[a] Beidou Feng,[a] Ge Wang,[b] Jingqiang Cui,[c] Lin Yang, [a,] * Kai Jiang,[a] and Hua Zhang [a,]*

[a] Key Laboratory of Green Chemical Media and Reactions, Ministry of Education; Collaborative Innovation Centre of Henan Province for Green Manufacturing of Fine Chemicals; Henan Key Laboratory of Organic Functional Molecule and Drug Innovation; School of Chemistry and Chemical Engineering Institution, Henan Normal University, Xinxiang 453007, China.

[b] School of Basic Medical Sciences, Xinxiang Medical University, Xinxiang 453007, China.

[c] Henan Key Laboratory of Medical Polymer Materials Technology and Application, Xinxiang 453007, China.

Contents

1. Experimental procedures

Solvents and reagents of A.R. grade were used in all this research column chromatograpy was used to purify compounds using silica gel (200-300 mesh). Cholinesterase, alkaline phosphatase, nuclease, phospholipase, sulfatase, sphingomyelinase, hepatic lipase, endothelial lipase, lipoprotein lipase, lysosomal acid lipase, acid cholesteryl ester hydrolase were obtained from Sigma Chemical Co. (USA). Doubly purified water was used in all experiments, which was prepared using by a Milli-Q system. Stock solutions of **HBT-ASD-1**, **HBT-ASD-2**, **HBT-ASD-3**, **HBT-ASD-4** and intermediate products were used in spectrographic determination and cell experiments. NMR spectra were obtained using an Avance 400 or 600 MHz spectrometer (Bruker Co., Switzerland). Ultra-high-resolution electro-spray time-of-flight mass spectrometry (Compact) was used to measure the molecular mass. BD FACSCanto II (USA) was used to sort cells in flow cytometic analysis.

1.1 Spectrographic determination in vitro

A cintra 2020 spectrophotometer (GBC Australia) and the fluoromax-4 spectrophotometer (HORIBA-PLUS-C, USA) were used to measure absorption spectra and fluorescence spectra, respectively. In all spectral experiments, the final solutions contained < 5.0‰ DMSO. Each experiment was carried out in five replicates (n = 5). The relative fluorescence quantum yields were determined using Rhodamine B (Φ_F = 0.97 in methanol) by the following equation:

$$\Phi_x=\Phi_s\ (F_x/\ F_s)(A_s/\ A_x)(\lambda_{exs}/\lambda_{exx})(\ n_x/\ n_s)^2 \qquad (1)$$

where Φ represents quantum yield; F is the integrated area under the corrected emission spectrum; A is absorbance at the excitation wavelength; λ_{ex} is the excitation wavelength; n is the refractive index of the solution (because of the low concentrations of the solutions, 10^{-7}-10^{-8} mol/L, the refractive indices of the solutions were replaced with those of the solvents); and the subscripts x and s refer to the unknown and the standard, respectively. The detection limit was calculated by three times the standard deviation divided by the slope of the calibration curve. The data were obtained from replicate experiments (n = 5).

1.2 Photostability in solution

HBT-ASD-1, **HBT-ASD-2**, **HBT-ASD-3** and **HBT-ASD-4** (5.0 μM) were dissolved in PBS buffer (pH 7.4) at 25 ℃, respectively. The solutions were irradiated by a 500W iodine-tungsten lamp situated 250 mm away for 7 h. An aqueous solution of sodium nitrite (50 g/L) was placed between the samples and the lamp as a light filter (to cut off the light shorter than 400 nm) and as a heat filter. The photostabilities were expressed in terms of remaining absorption (%) calculated from the changes of absorbance at the absorption maximum before and after irradiation by iodine-tungsten lamp. The absorbance was determined. The data were obtained from replicate experiments (n = 5).

1.3 Quantum Calculations

All the quantum chemical calculations were done with the Gaussian 16 suite. The geometry optimizations of the **HBT-ASD-2** was performed using density functional theory (DFT) with Becke's three- parameter hybrid exchange function with Lee-Yang-Parrgradient-corrected correlation functional (B3-LYP functional).

Gaussian 16 was used in quantum chemical, and the work of Han was as reference for setting up calculation parameter[S1]. The density functional theory (DFT)[S2] with B3-LYP and B3LYP-D3 functional were used in the geometry optimizations of the dyes. And 6-31G* basis set was utilized. No constraints to bonds/angles/dihedral angles were applied in the calculations and all atoms were free to optimize.

1.4 Cell Culture

HepG 2 cell lines, 7702 cell lines and the hemocyte were obtained from the Chinese Academy of Medical Sciences. The red-free Dulbecco's Modified Eagle's Medium (DMEM, WelGene) and eagle's minimum essential medium (MEM, WelGene) supplemented with penicillin/streptomycin and 10 % fetal bovine serum (FBS; Gibco) were used to culture cells in a CO_2 incubator at 37 ℃. One day before imaging, the cells mentioned above were seeded into confocal dishes with well glass bottom (MatTek, 1# glass, 0.13-0.16 mm).

They were incubated at 37 ℃ in 5.0 wt %/vol CO_2 for 24 h. And then, the cells were incubated with HBT-NA at a certain concentration.

1.5 Cytotoxicity

HepG 2 cell lines, 7702 cell lines and the hemocyte were prepared for cell viability studies in 96-well plates (1×10^5 cells per well that were incubated in 100 μL). The cells were incubated for an additional 24 h with dyes **HBT-ASD-1, HBT-ASD-2, HBT-ASD-3** and **HBT-ASD-4** in different concentrations. Subsequently, 100 μL of 3-(4,5-dimethylthiazol-2-yl)-2,5-diphenyltetrazolium bromide (MTT, Sigma Chemical Co. U.S.A.) was added into each well, followed by further incubation for 4 h at 37 ℃. The DMEM was removed and DMSO (200 μL/well) added to dissolve the reddish-blue crystals. Optical density (OD) was determined by a microplate reader (Spectra Max M5, Molecular Devices) at 570 nm with subtraction of the absorbance of the cell-free blank volume at 630 nm. The results from the six individual experiments were averaged. The relative cell viability (100%) was calculated using the following equation:

$$\text{Cell viability (\%)} = (OD_{dye}\text{-}OD_{k\text{-}dye})/(OD_{ctrl}\text{-}OD_{k\text{-}ctrl}) \times 100 \quad (2)$$

1.6 Flow cytometry

The pure and highly immunoreactive neutrophil granulocyte, lymphocyte, monocyte, alkaline granulocyte and acid granulocyte were incubated with **HBT-ASD-1, HBT-ASD-2, HBT-ASD-3** and **HBT-ASD-4** (5.0 μM) for 30 min, then the cells were washed. The cells were then dispersed into PBS solution at level of 10,000 cells/500 μL. Samples were analyzed with the laser (365 nm) on a flow cytometer (BD FACSCanto II, USA). The average fluorescence intensity in 10,000 cells was obtained and analyzed with BD FACSDiva software. The excitation wavelength for the blue channel: 365 nm, blue channel: 410-460 nm, green channel: 500-550 nm.

2. The synthesis of HBT-ADSs

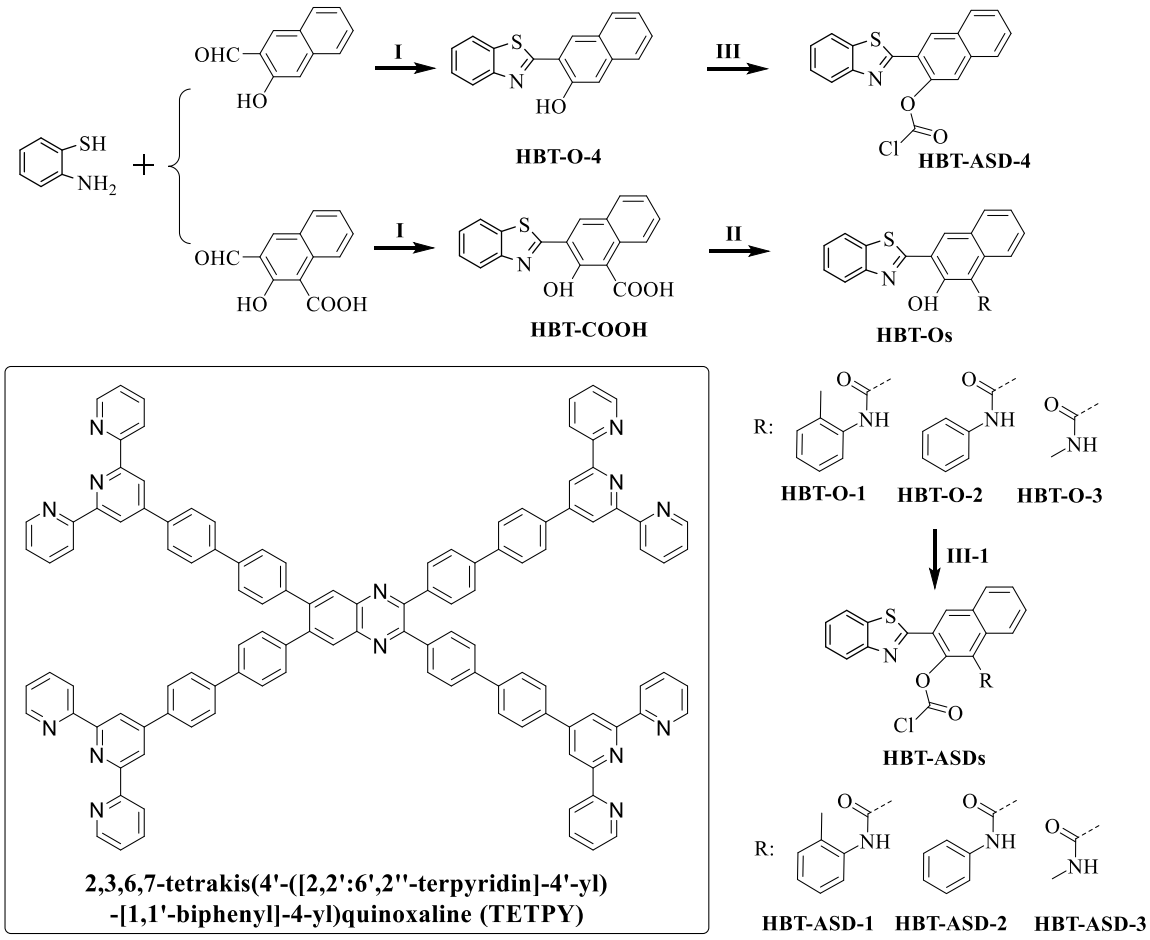

Scheme S1. The molecular structure of HBT-ASDs derivants

3-(benzo[*d*]thiazol-2-yl)-2-hydroxy-1-naphthoic acid (intermediate product, HBT-COOH)

The reference method (J. Org. Chem. **2020**, 85, 13906-13919) was used to synthesize separate and purify the intermediate product **HBT-COOH** (3-(benzo[*d*]thiazol-2-yl)-2-hydroxy-1-naphthoic acid, intermediate product). 2-aminobenzenethiol (2.0 mmol, 250 mg), 3-formyl-2-hydroxy-1-naphthoic acid (2.5 mmol, 540 mg) were mixed in EtOH (2.0 mL). 2,3,6,7-tetrakis(4'-([2,2':6',2''-terpyridin]-4'-yl)-[1,1'-biphenyl]-4-yl)quinoxaline (TETPY, 0.1 mol %, 4.0 mg of TETPY dissolved in 800 μL of DMSO and 1200 μL of distilled water) was as a photocatalyst under visible light irradiation using air as an oxidant. The resulting solution (500 μL) was used as the photocatalyst for the **Reaction I-1**: 16 W white LED as the irradiation source at the room temperature in aerial conditions for 40 min. Isolated form of TETPY (1.0 mg). **HBT-COOH** (3-(benzo[*d*]thiazol-2-yl)-2-hydroxy-1-naphthoic acid) was obtained 480 mg (Yield 75%). ^{1}H NMR (600 MHz, DMSO-d6) δ: 13.47 (s, 1H),

8.97 (d, *J* = 5.5 Hz, 1H), 8.33 (d, *J* = 5.3 Hz, 1H), 8.25 (d, *J* = 5.4 Hz, 1H), 8.13 (t, *J* = 4.9 Hz, 1H), 8.08 (dd, *J* = 10.2, 5.4 Hz, 2H), 8.03 (d, *J* = 5.8 Hz, 1H), 7.95 (d, *J* = 5.3 Hz, 1H), 7.88 (d, *J* = 5.7 Hz, 1H); ^{13}C NMR (151 MHz, DMSO-d6) *δ*: 170.70, 167.96, 153.55, 150.20, 134.27, 131.43, 127.83, 126.90, 126.19, 125.42, 124.69, 123.60, 123.47, 122.26, 121.46, 120.78, 118.85, 109.22. HRMS: m/z calcd for $C_{18}H_{11}NO_3S$-2H: 319.0303, found: 319.0317.

4-(benzo[*d*]thiazol-2-yl)-3-hydroxy-*N*-(*o*-tolyl)-2-naphthamide (intermediate product, HBT-O-1)

To a solution of **HBT-COOH** (0.36 mmol, 115mg) in 20 mL CH_2Cl_2, *o*-toluidine (0.42 mmol, 45mg), 1-(3-dimethylaminopropyl)-3-ethylcarbodiimide hydrochloride (EDCl) (0.70 mmol, 134mg), and 4-dimethylaminopyridine (DMAP) (0.70 mmol, 85mg) were added. The solution was stirred at room temperature under nitrogen for 24 h and then concentrated. The residue was purified by silica gel column chromatography by using CH_2Cl_2/CH_3OH 60:1 (v/v) as eluent, affording **HBT-O-1** (0.25 mmol, 105 mg). Yield 69 %. ^{1}H NMR (600 MHz, DMSO-d6) *δ*: 13.84 (s, 1H), 8.97 (d, *J* = 5.5 Hz, 1H), 8.58 (s, 1H), 8.33 (d, *J* = 5.3 Hz, 1H), 8.25 (d, *J* = 5.4 Hz, 1H), 8.13 (t, *J* = 4.9 Hz, 1H), 8.08 (dd, *J* = 10.2, 5.4 Hz, 2H), 8.03 (d, *J* = 5.8 Hz, 1H), 7.95 (d, *J* = 5.3 Hz, 1H), 7.88 (d, *J* = 5.7 Hz, 1H), 7.26 (t, *J* = 4.9 Hz, 1H), 7.21 (dd, *J* = 10.2, 5.4 Hz, 2H), 7.16 (d, *J* = 5.8 Hz, 1H), 3.55 (s, 3H); ^{13}C NMR (151 MHz, DMSO-d6) *δ*: 170.70, 167.96, 153.55, 150.20, 134.27, 132.88, 131.92, 131.43, 130.39, 130.12, 129.03, 128.34, 127.83, 126.90, 126.19, 125.42, 124.69, 123.60, 123.47, 122.26, 121.46, 120.78, 118.85, 109.22, 22.00. HRMS: m/z calcd for $C_{25}H_{18}N_2O_2S$-H: 409.1011, found: 409.1025.

4-(benzo[*d*]thiazol-2-yl)-3-hydroxy-*N*-phenyl-2-naphthamide (intermediate product, HBT-O-2)

The synthesis and purification methods are similar to those of **HBT-O-1**. The residue was purified by silica gel column chromatography by using CH_2Cl_2/CH_3OH 60:1 (v/v) as eluent, affording **HBT-O-2** (0.27 mmol, 110 mg). Yield 73%. ^{1}H NMR (600 MHz, DMSO-d6) *δ*: 13.47 (s, 1H), 8.97 (d, *J* = 5.5 Hz, 1H), 8.80 (s, 1H), 8.33 (d, *J* = 5.3 Hz, 1H), 8.25 (d, *J* = 5.4 Hz, 1H), 8.13 (t, *J* = 4.6 Hz, 1H), 8.08 (dd, *J* = 10.2, 5.4 Hz, 2H), 8.03 (d, *J* = 5.8 Hz, 1H), 7.95 (d, *J* = 5.3 Hz, 1H), 7.88 (d, *J* = 5.7 Hz, 1H), 7.60 (d, *J* = 5.3 Hz, 2H), 7.11 (t, *J* = 4.9 Hz, 2H), 7.02 (t, *J* = 4.9 Hz, 1H); ^{13}C NMR (151 MHz, DMSO-d6) *δ*: 170.57, 167.84, 153.42, 150.07, 134.18, 131.49, 127.71, 126.78, 126.06, 125.30, 124.57, 123.84, 123.47, 123.35, 122.82, 122.44, 122.13, 121.33, 120.66, 120.23, 119.46, 118.73, 117.72, 109.02. HRMS: m/z calcd for $C_{24}H_{16}N_2O_2S$-H: 395.0854, found: 395.0848.

4-(benzo[*d*]thiazol-2-yl)-3-hydroxy-*N*-methyl-2-naphthamide (intermediate product, HBT-O-3)

The synthesis and purification methods are similar to those of **HBT-O-1**. The residue was purified by silica gel column chromatography by using CH_2Cl_2/CH_3OH 60:1 (v/v) as eluent, affording **HBT-O-3** (0.26 mmol, 84 mg). Yield 72%. ^{1}H NMR (600 MHz, DMSO-d6) *δ*: 13.47 (s, 1H), 8.97 (d, J = 5.5 Hz, 1H), 8.33 (d, J = 5.3 Hz, 1H),

8.25 (d, J = 5.4 Hz, 1H), 8.13 (t, J = 4.9 Hz, 1H), 8.08 (dd, J = 10.2, 5.4 Hz, 1H), 8.03 (d, J = 5.8 Hz, 2H), 7.95 (d, J = 5.3 Hz, 1H), 7.88 (d, J = 5.7 Hz, 1H), 2.17 (s, 3H); ^{13}C NMR (151 MHz, DMSO-d6) δ: 170.39, 167.65, 153.17, 149.93, 134.00, 131.13, 127.53, 126.60, 125.88, 125.11, 124.39, 123.29, 123.17, 121.95, 121.15, 120.48, 118.55, 108.77, 25.77. HRMS: m/z calcd for $C_{19}H_{14}N_2O_2S$-H: 333.0698, found: 333.0672.

1-(benzo[*d*]thiazol-2-yl)naphthalen-2-ol (intermediate product, HBT-O-4)

2-aminobenzenethiol (2.0 mmol, 250 mg), 3-hydroxy-2-naphthaldehyde (2.5 mmol, 430 mg) were mixed in EtOH (2.0 mL). The synthesis and purification methods are similar to those of **HBT-COOH**. **HBT-O-4** (3-(benzo[d]thiazol-2-yl)naphthalen-2-ol) was obtained 227 mg (Yield 82%). ^{1}H NMR (600 MHz, DMSO-d6) δ: 14.41 (s, 1H), 8.97 (d, *J* = 5.5 Hz, 1H), 8.33 (d, *J* = 5.3 Hz, 1H), 8.25 (d, *J* = 5.4 Hz, 1H), 8.13 (t, *J* = 4.9 Hz, 1H), 8.08 (dd, *J* = 10.2, 5.4 Hz, 2H), 8.03 (d, *J* = 5.8 Hz, 1H), 7.95 (d, *J* = 5.3 Hz, 1H), 7.88 (d, *J* = 5.7 Hz, 1H), 7.63 (d, *J* = 5.3 Hz, 1H); ^{13}C NMR (151 MHz, DMSO-d6) δ: Unknown NMR (400 MHz,) δ 167.96, 153.55, 150.20, 134.27, 131.43, 127.83, 126.90, 126.19, 125.42, 124.69, 123.60, 123.47, 122.26, 121.46, 120.78, 118.85, 109.18. HRMS: m/z calcd for $C_{17}H_{11}NOS$-H: 276.0483, found: 276.0497.

1-(benzo[*d*]thiazol-2-yl)-3-(*o*-tolylcarbamoyl)naphthalen-2-yl carbonochloridate (product, HBT-ASD-1)

The intermediate product (**HBT-O-1**, 0.36 mmol, 150 mg) and triethylamine (0.43 mmol, 43 mg) were dissolved in dichloromethane and stirred under N_2 for 10 min. Acetyl chloride (0.42 mmol, 33 mg) dissolved in dichloromethane and was added dropwise into the mixture at 0 ^{o}C. After complete addition, the solvent stirred for 2.0 h at room temperature, and monitored by TLC. When the reaction was complete, 80 mL of water was added into the mixture to quench the reaction. The mixture was separated by extraction using petroleum ether three times, and the organic phase was collected. Then, the crude product **HBT-ASD-1** was obtained after the solvent was removed under reduced pressure. Column chromatography using silica gel was used to purify **HBT-ASD-1** using petroleum ether/Ethyl Acetate (100:1 to 30:1, v/v) as eluent. **HBT-ASD-1** (1-(benzo[*d*]thiazol-2-yl)-3-(*o*-tolylcarbamoyl)naphthalen-2-yl carbonochloridate) was obtained at Yield 65%. ^{1}H NMR (600 MHz, DD) δ: 8.96 (d, J = 5.5 Hz, 1H), 8.57 (s, 1H), 8.32 (d, J = 5.3 Hz, 1H), 8.24 (d, J = 5.4 Hz, 1H), 8.12 (t, J = 4.9 Hz, 1H), 8.07 (dd, J = 10.2, 5.4 Hz, 2H), 8.02 (d, J = 5.8 Hz, 1H), 7.94 (d, J = 5.3 Hz, 1H), 7.87 (d, J = 5.7 Hz, 1H), 7.25 (t, J = 4.6 Hz, 1H), 7.20 (dd, J = 10.2, 5.4 Hz, 2H), 7.15 (d, J = 5.8 Hz, 1H), 3.55 (s, 3H). ^{13}C NMR (151 MHz, $CDCl_3$) δ: 170.70, 167.96, 153.55, 150.20, 134.27, 133.40, 132.88, 131.92, 131.43, 130.39, 130.12, 129.03, 128.34, 127.83, 126.90, 126.19, 125.42, 124.69, 123.60, 123.47, 122.26, 121.46, 120.78, 118.85, 109.32, 22.21. HRMS: m/z calcd for $C_{26}H_{17}ClN_2O_3S$: 472.0648, found: 472.0641.

1-(benzo[*d*]thiazol-2-yl)-3-(phenylcarbamoyl)naphthalen-2-yl carbonochloridate (product, HBT-ASD-2)

The synthesis and purification methods are similar to those of **HBT-ASD-1**. **HBT-ASD-2** (1-(benzo[*d*]thiazol-2-yl)-3-(phenylcarbamoyl)naphthalen-2-yl carbonochloridate) was obtained at Yield 63%. ^{1}H NMR (600 MHz, DD) δ: 8.97 (d, J = 5.5 Hz, 1H), 8.80 (s, 1H), 8.33 (d, J = 5.3 Hz, 1H), 8.25 (d, J = 5.4 Hz, 1H), 8.13 (t, J = 4.6 Hz, 1H), 8.08 (dd, J = 10.2, 5.4 Hz, 2H), 8.03 (d, J = 5.8 Hz, 1H), 7.95 (d, J = 5.3 Hz, 1H), 7.88 (d, J = 5.7 Hz, 1H), 7.60 (d, J = 5.3 Hz, 2H), 7.11 (t, J = 4.9 Hz, 2H), 7.02 (t, J = 4.9 Hz, 1H); ^{13}C NMR (151 MHz, $CDCl_3$) δ: 170.57, 167.84, 153.42, 150.07, 134.15, 131.31, 129.96, 127.71, 126.78, 126.06, 125.30, 124.57, 123.84, 123.47, 123.35, 122.82, 122.44, 122.13, 121.33, 120.66, 120.23, 119.46, 118.73, 117.72, 108.96. HRMS: m/z calcd for $C_{25}H_{15}ClN_2O_3S$: 458.0492, found: 458.0486.

1-(benzo[*d*]thiazol-2-yl)-3-(methylcarbamoyl)naphthalen-2-yl carbonochloridate (product, HBT-ASD-3)

The synthesis and purification methods are similar to those of **HBT-ASD-1**. **HBT-ASD-3** (1-(benzo[*d*]thiazol-2-yl)-3-(methylcarbamoyl)naphthalen-2-yl carbonochloridate) was obtained at Yield 65%. ^{1}H NMR (600 MHz, DD) δ: 8.98 (d, J = 5.5 Hz, 1H), 8.33 (d, J = 5.3 Hz, 1H), 8.25 (d, J = 5.4 Hz, 1H), 8.13 (t, J = 4.9 Hz, 1H), 8.08 (dd, J = 10.2, 5.4 Hz, 1H), 8.03 (d, J = 5.8 Hz, 2H), 7.95 (d, J = 5.3 Hz, 1H), 7.88 (d, J = 5.7 Hz, 1H), 2.17 (s, 3H); ^{13}C NMR (151 MHz, DMSO-d6) δ: Unknown NMR (400 MHz,) δ 170.56, 167.72, 153.39, 149.84, 133.96, 131.09, 128.06, 127.42, 126.52, 125.98, 125.06, 124.52, 123.41, 123.33, 121.95, 121.33, 120.48, 118.50, 108.79, 25.68. HRMS: m/z calcd for $C_{20}H_{13}ClN_2O_2S$: 396.0335, found: 396.0345.

3-(benzo[*d*]thiazol-2-yl)naphthalen-2-yl carbonochloridate (product, HBT-ASD-4)

The synthesis and purification methods are similar to those of **HBT-ASD-1**. **HBT-ASD-4** (3-(benzo[*d*]thiazol-2-yl)naphthalen-2-yl carbonochloridate) was obtained at Yield 74%. ^{1}H NMR (600 MHz, DMSO-d6) δ: 8.97 (d, J = 5.5 Hz, 1H), 8.33 (d, J = 5.3 Hz, 1H), 8.25 (d, J = 5.4 Hz, 1H), 8.13 (t, J = 4.9 Hz, 1H), 8.08 (dd, J = 10.2, 5.4 Hz, 2H), 8.03 (d, J = 5.8 Hz, 1H), 7.95 (d, J = 5.3 Hz, 1H), 7.88 (d, J = 5.7 Hz, 1H), 7.63 (d, J = 5.3 Hz, 1H); ^{13}C NMR (151 MHz, DMSO-d6) δ: 167.96, 153.62, 150.14, 137.62, 134.27, 131.43, 127.83, 126.90, 126.11, 125.49, 124.69, 123.60, 123.53, 122.26, 121.46, 120.78, 118.85, 109.28. HRMS: m/z calcd for $C_{18}H_{10}ClNO_2S$: 339.0121, found: 339.0133.

Based on such a design strategy, **HBT-ASDs** derivants can emit the differential fluorescence signal that is simultaneously activated by the **NAS-DCE** and pH. Then, the three different kinds of granulocytes can be separated and sorted from blood by such differential and sensitive fluorescence signals, and the activity of **NAS-DCE** in different granulocytes can be monitored in real-time. The molecular structure (**Scheme 1**), synthetic route (**Scheme S1**), structural characterisation and properties of **HBT-ASDs** derivants and the intermediate are listed in the supporting information.

3. The optical data and the absorption spectra of HBT-ASDs derivants

The spectral data (*i.e.* the absorption spectra, the emission spectra, the molar extinction coefficient ε and the fluorescence quantum yield Φ) of **HBT-ASDs** derivants for the **NAS-DCE** were obtained under different pH conditions in the PBS buffer (see the **Fig. 1**, and **Table S1**). **HBT-ASDs** derivants presented different response signals. **HBT-ASD-2** was used as the typical molecule to explain the spectral characterisation of **HBT-ASDs** derivants.

Table S1. The optical data of HBT-ASDs derivants and its recognition derivatives

	HBT-ASD-1			**HBT-ASD-2**			**HBT-ASD-3**			**HBT-ASD-4**		
Only Dyes in Buffer Solution												
pH of solution	5.0	7.4	10	5.0	7.4	10	5.0	7.4	10	5.0	7.4	10
λ_{ex}/nm	359	358	357	365	365	367	343	345	344	342	343	343
ε / M^{-1} cm^{-1} $\times 10^4$	0.943	0.912	0.955	1.124	1.119	1.131	1.023	1.014	1.019	1.101	1.045	1.019
λ_{em}/nm	431	432	432	435	438	439	420	423	427	428	427	429
Φ	0.027	0.023	0.021	0.067	0.063	0.071	0.12	0.11	0.12	0.095	0.089	0.086
Dyes Encountered with the NAS-DCE (20 unit) in Buffer Solution												
pH of solution	5.0	7.4	10	5.0	7.4	10	5.0	7.4	10	5.0	7.4	10
λ_{ex}/nm	359	358	357	375	376	389	343	345	344	342	343	343
ε / M^{-1} cm^{-1} $\times 10^4$	0.953	0.923	0.971	1.698	1.719	1.705	1.023	1.014	1.019	1.101	1.045	1.019
λ_{em}/nm	431	432	432	545/438	438	438	421	423	425	428	427	429
Φ	0.035	0.037	0.033	0.37	0.15	0.59	0.12	0.11	0.12	0.095	0.089	0.086
Form of Fluorescence Intensity	—	—	—	$F_{5.0\text{-}545}/F_{5.0\text{-}438}$	$F_{7.4\text{-}438}/F^0_{7.4\text{-}438}$	$F_{10\text{-}438}/F^0_{10\text{-}438}$	—	—	—	—	—	—

Φ fluorescence quantum yield; ε Molar extinction coefficient.

4. The time response of HBT-ASDs derivants for NAS-DCE

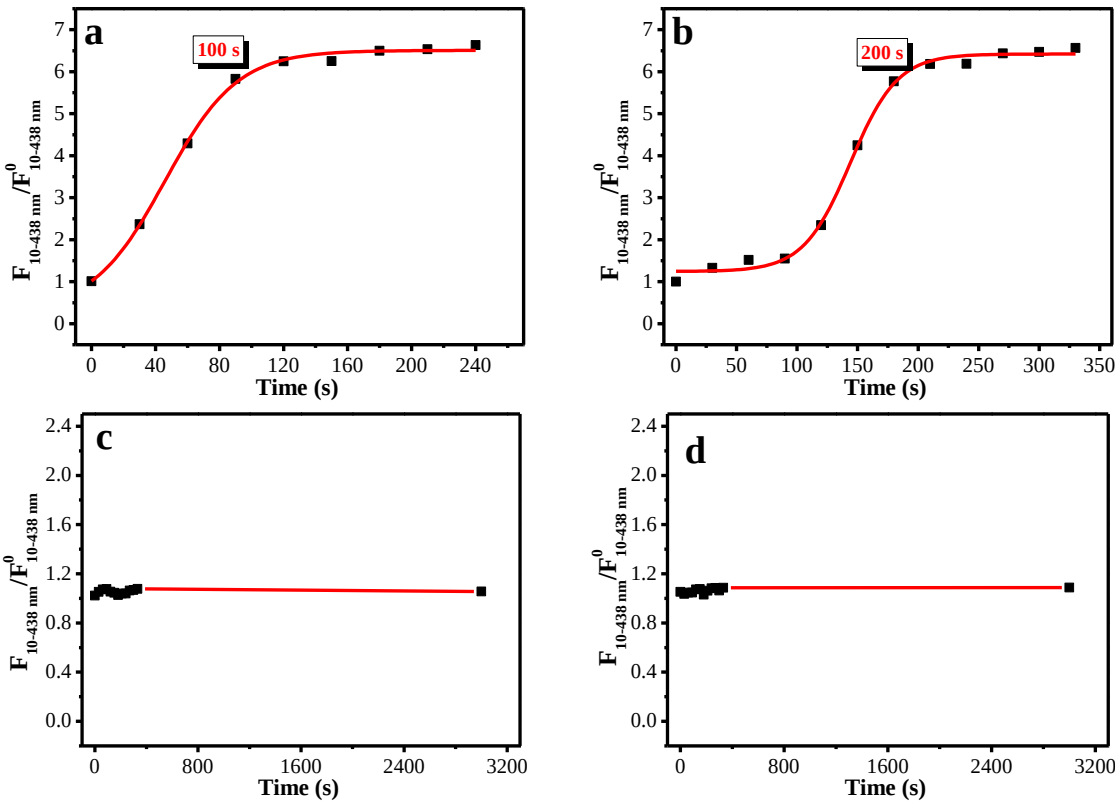

Figure S1. The reaction profile of **HBT-ASD-2** (5.0 μM, a), **HBT-ASD-1** (5.0 μM, b), **HBT-ASD-3** (5.0 μM, c) and **HBT-ASD-4** (5.0 μM, d) for **NAS-DCE** (15.0 unit) in PBS buffer solutions (pH = 10).

5. The selective experiment of HBT-ASDs derivants

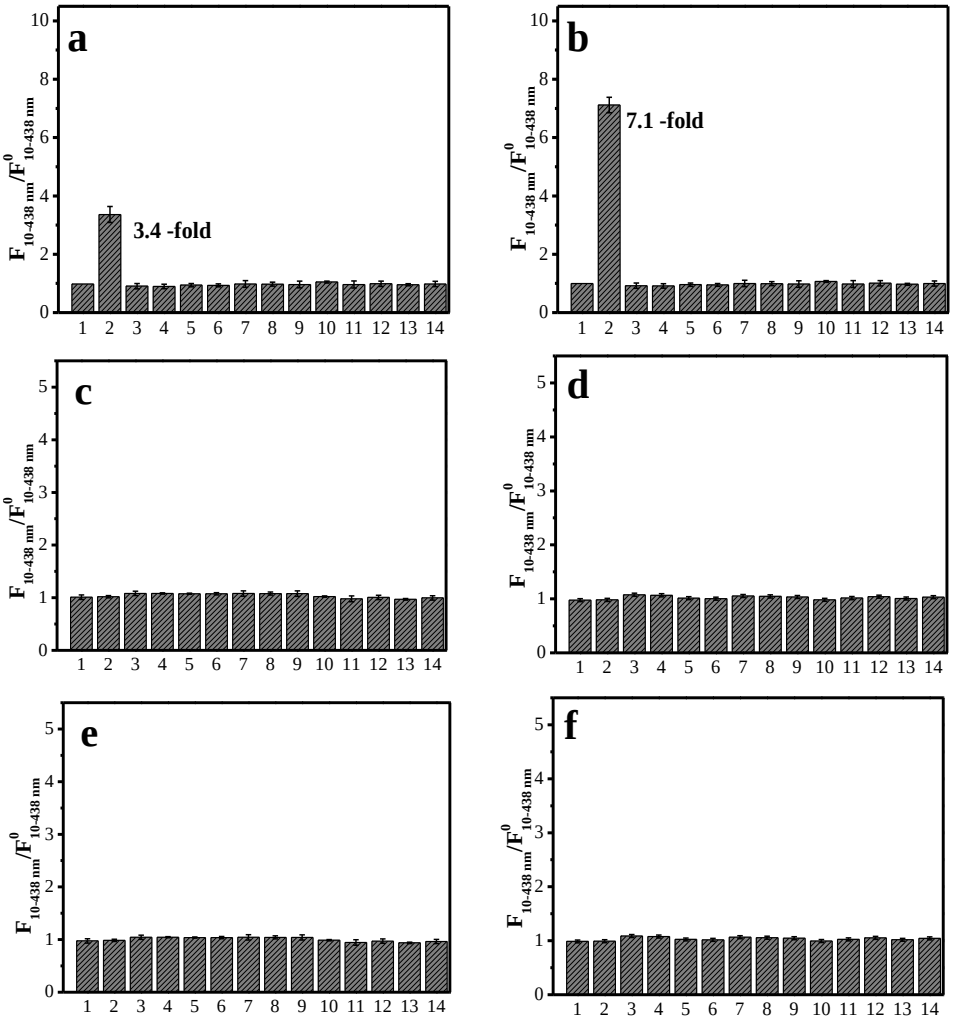

Figure S2. Selective experiment of **HBT-ASD-1** (a, c and e) and **HBT-ASD-2** (b, d and f) in pH = 10. (a) and (b) The interferent lipases: 1, control; 2, NAS-DCE; 3, naphthalene acetate esterase; 4, cholinesterase; 5, alkaline phosphatase; 6, nuclease; 7, phospholipase; 8, sulfatase; 9, sphingomyelinase; 10, hepatic lipase; 11, endothelial lipase; 12, lipoprotein lipase; 13, lysosomal acid lipase; and 14, acid cholesteryl ester hydrolase. (c) and (d) The interferent ions: 1. Control, 2. Ag^+ (0.10 mM), 3. Al^{3+} (0.10 mM), 4. NO_3^- (0.30 mM), 5. Ni^{2+} (0.10 mM), 6. Cl^- (0.20 mM), 7. Mg^{2+} (0.10 mM), 8. SO_4^{2-} (0.10 mM), 9. CO_3^{2-} (0.050 mM), 10. Na^+ (0.10 mM), 11. K^+ (0.10 mM), 12. Ca^{2+} (0.10 mM), 14. $H_2PO_4^-$ (0.10 mM). (e) and (f) The interferent bioactive small molecules: 1, control; 2, arginine; 3, glycine; 4, aspartic acid; 5, 5-hydroxytryptamine; 6, catecholamine; 7, glutamic acid; 8, aminobutyric acid; 9, H_2S; 10, NO_2; 11, NO; 12, H_2O_2 ; 13, $ONOO^-$; and 14, $O_2^{\cdot-}$. Excitation wavelength = 365 nm. emission wavelength = 438 nm. **HBT-ASD-1** and **HBT-ASD-2**: 5.0 μM. Data were obtained from replicate experiments (n = 5).

6. The pH-stability of HBT-ASDs derivants and their product of hydrolysis

No any influence on the fluorescent signal was observed when the pH of phosphate buffer was varied from 3.0-11.0. Such kind of pH-stability of **HBT-ASD-1** and **HBT-ASD-2** ensures that it can provide a stable response signal for the ultra-sensitive detection of the enzyme activities.

The spectral responses of hydrolysis products—**HBT-O-1** and **HBT-O-2** for the different pH (5.0, 7.4 and 10) were detected. The results (**Figure S3c** and **S3d**) were consistent with spectral response of **HBT-ASD-1** and **HBT-ASD-2** for **NAS-DCE** (15.0 unit) and pH (5.0, 7.4 and 10), which proved that the pH sensitivity is coming from the hydrolysis products.

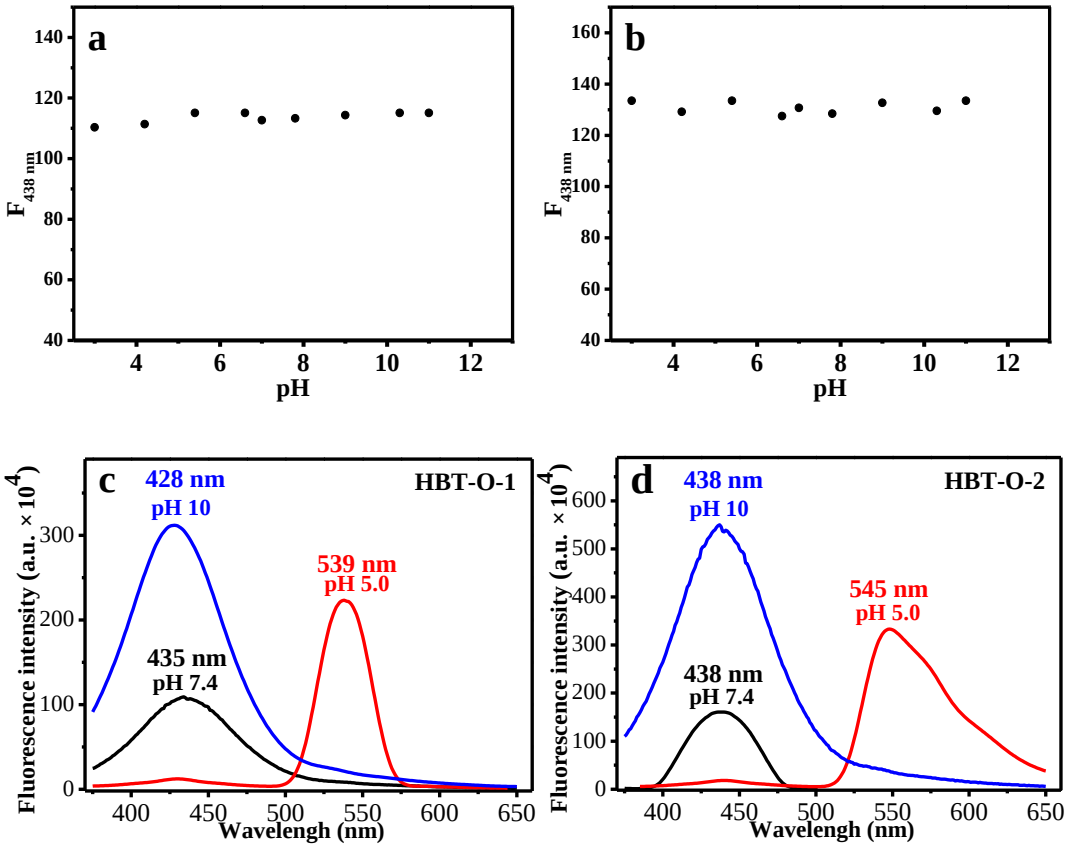

Figure S3. The pH-stability of **HBT-ASD-1** (5.0 μM) and **HBT-ASD-2** (5.0 μM) in pH range from 3.0 to 11.0. Excitation wavelength = 365 nm. emission wavelength = 438 nm. The spectral response of **HBT-O-1** (5.0 μM, c) and **HBT-O-2** (5.0 μM, d) under different pH (5.0, 7.4 and 10). Data were obtained from replicate experiments (n = 5).

7. Biocompatibility of HBT-ASDs derivants

Prior to the cell assay, the biocompatibility of **HBT-ASD-1, HBT-ASD-2, HBT-ASD-3** and **HBT-ASD-4** including photostability, cell toxicity, water solubility and so on, were evaluated by fluorescence intensity as the evaluation parameter, respectively.

7.1 The photostability under irradiation by iodine-tungsten lamp in PBS buffer

HBT-ASD-1, HBT-ASD-2, HBT-ASD-3 and **HBT-ASD-4** (5.0 μM) retained more than 98% of the fluorescence intensity in PBS buffer after they were continuously irradiated by an iodine-tungsten lamp for 6.0 h. The photostability of **HBT-ASD-1, HBT-ASD-2, HBT-ASD-3** and **HBT-ASD-4** ensures that it can provide a stable response signal for the ultra-sensitive detection of the enzyme activity and the real-time precise typing of lymphocytes.

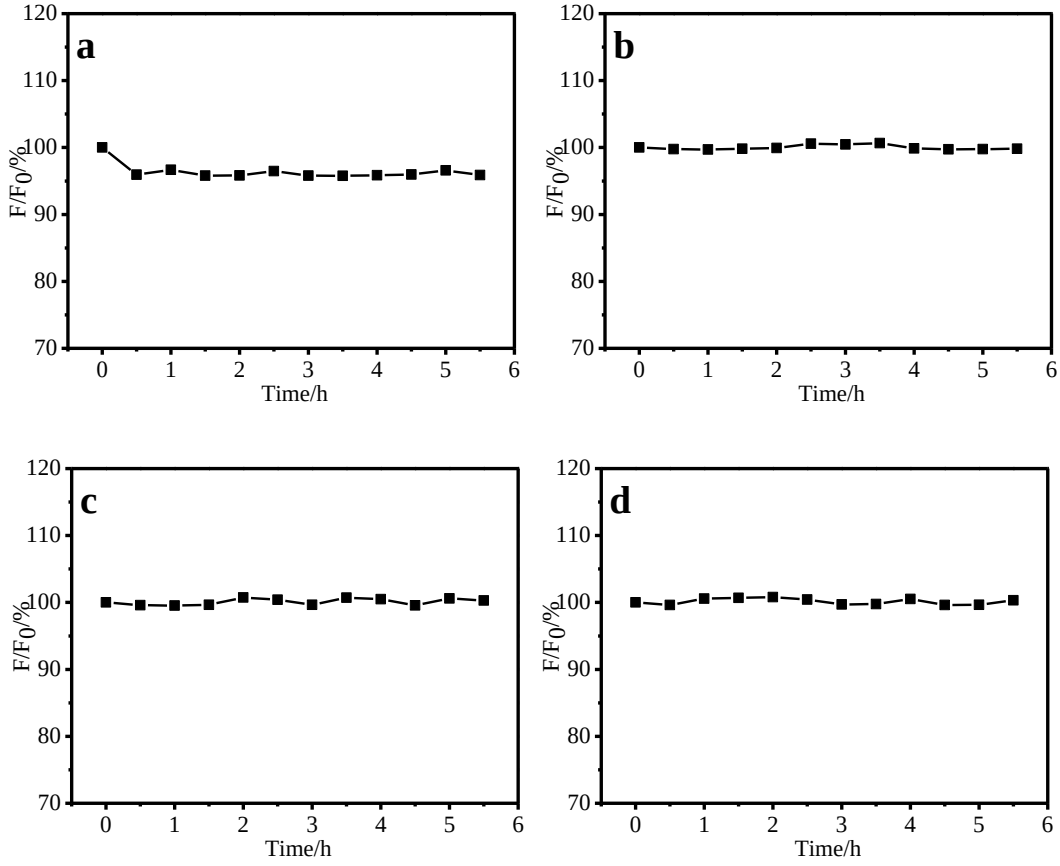

Figure S4. The photostability of **HBT-ASD-1** (a), **HBT-ASD-2** (b), **HBT-ASD-3** (c) and **HBT-ASD-4** (d) in PBS buffer (pH 7.4) at 25 ℃. Iodine-tungsten lamp: 500W. Excitation wavelength = 365 nm. Emission wavelength = 438 nm. The concentration of **HBT-ASD-1**, **HBT-ASD-2**, **HBT-ASD-3** and **HBT-ASD-4** are 5.0 μM.

7.2 The biological photostability of HBT-NA in cells

HBT-ASD-1, HBT-ASD-2, HBT-ASD-3 and **HBT-ASD-4** (5.0 μM) retained more than 99 % of the fluorescence intensity in living cell after being continuously irradiated by a laser at 405 nm (initial power = 2.6 mM) for 6.0 h. Such biological photostability of **HBT-ASD-1, HBT-ASD-2, HBT-ASD-3** and **HBT-ASD-4** ensures that it can provide a stable response signal for the ultra-sensitive detection of the enzyme activity and the real-time precise typing of lymphocyte.

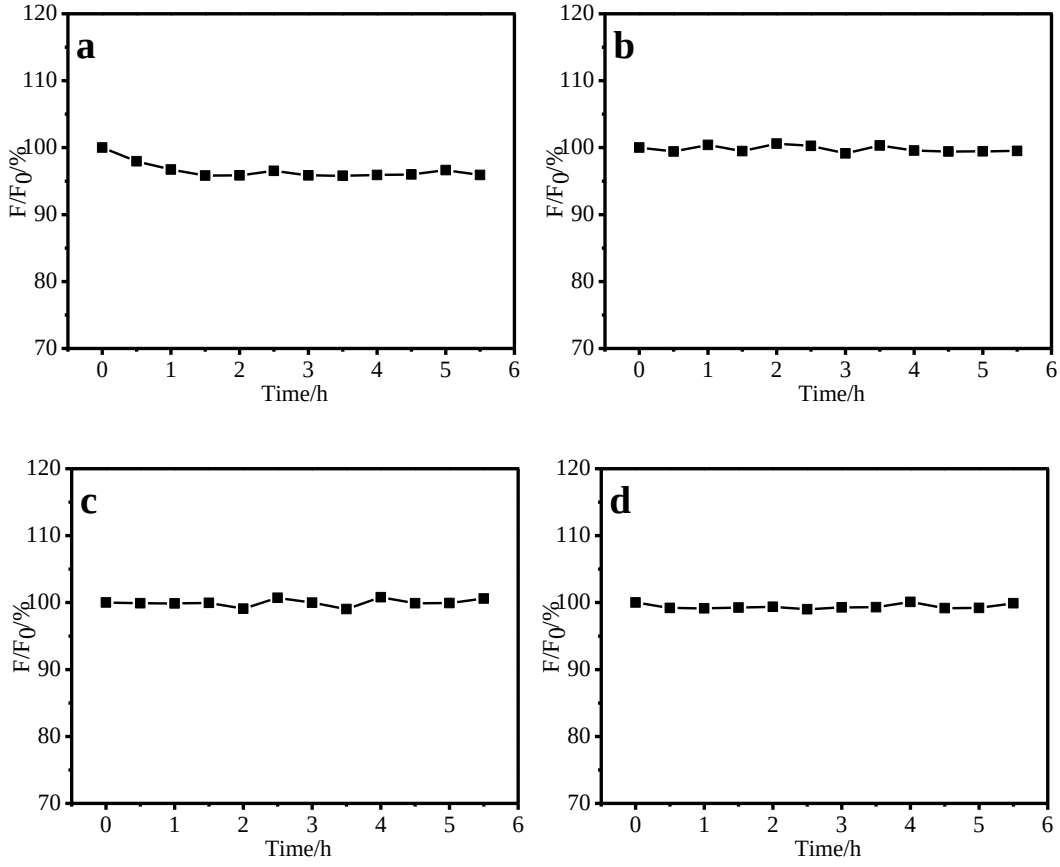

Figure S5. The biological photostability of **HBT-ASD-1** (a), **HBT-ASD-2** (b), **HBT-ASD-3** (c) and **HBT-ASD-4** (d) in cell. Excitation wavelength = 405 nm. Emission wavelength = 410-460 nm. The concentration of **HBT-ASD-1**, **HBT-ASD-2**, **HBT-ASD-3** and **HBT-ASD-4** are 5.0 μM.

7.3 The cell toxicity of HBT-ASD-1, HBT-ASD-2, HBT-ASD-3 and HBT-ASD-4

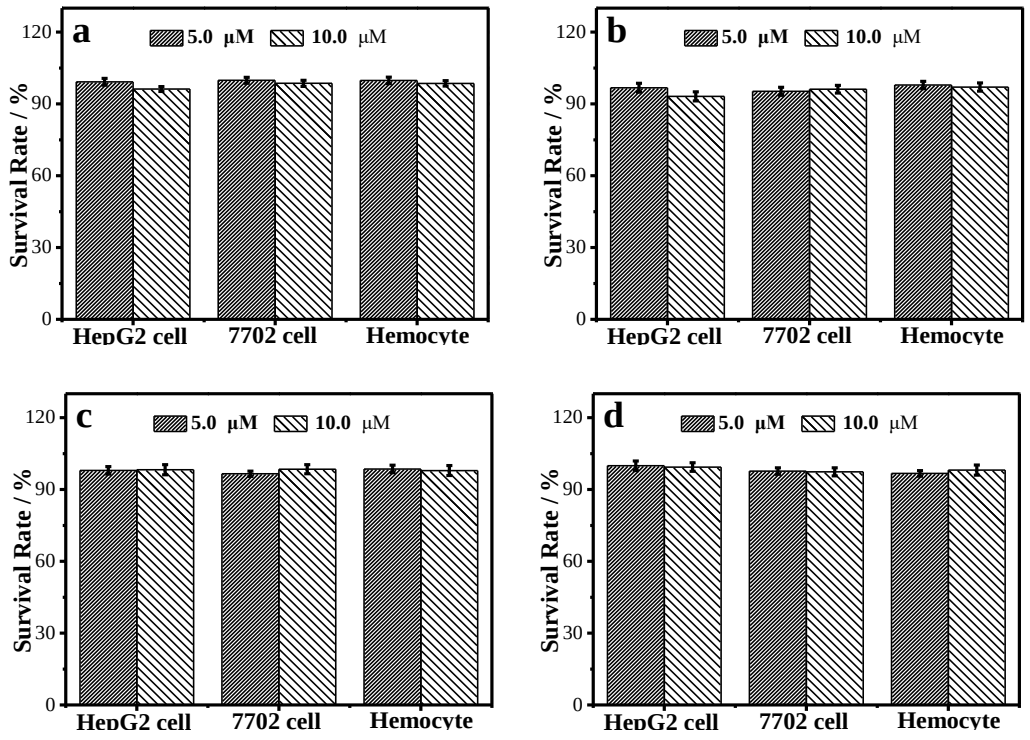

Figure S6. The cell toxicity of **HBT-ASD-1** (a), **HBT-ASD-2** (b), **HBT-ASD-3** (c) and **HBT-ASD-4** (d) for HepG2 cells, 7702 cells and hemocytes. The concentration of **HBT-ASD-1**, **HBT-ASD-2**, **HBT-ASD-3** and **HBT-ASD-4** are 5.0 μM and 10.0 μM.

Furthermore, **HBT-ASD-1** presented similar spectral changes (**Table S1** and **Fig. S1b**). However, compared with **HBT-ASD-2**, **HBT-ASD-1** presented a certain performance difference in fluorescence quantum yield, response speed and so on. This was due to the introduction of group labelled red into the **HBT-ASDs** derivants (**Scheme 1**), which led to the difference in molecular steric hindrance. These groups limited the occurrence of the ESIPT process in **HBT-ASD-1**. However, **HBT-ASD-3** and **HBT-ASD-4** did not show any spectral changes for **NAS-DCE** at any pH. **HBT-ASD-3** and **HBT-ASD-4** do not contain the specific recognition group for **NAS-DCE**, and the specific recognition response hydrolysis reaction cannot be initiated.[3-5] Finally, the ESIPT process was always blocked.

Selectivity, pH stability, cytotoxicity, photostability and so on, which were the important factors affecting performance during the cell sorting and real-time monitoring, were successively evaluated. **Fig. S2a** and **S2b** indicated that the response signals of **HBT-ASD-1** and **HBT-ASD-2** were consistent with the blank group, when they encountered other lipases (hepatic lipase, endothelial lipase, lipoprotein lipase, phospholipase, lysosomal acid lipase and so on) and esterase (such as cholinesterase, naphthalene acetate esterase, sulfatase, sphingomyelinase and so on) in the organisms. The same results were obtained n in the presence of different ions (**Fig. S2c** and **S2d**) and bioactive small molecules (**Fig. S2e** and **S2f**). In the absence of lipase in the organisms, the output signals of **HBT-ASD-1** and **HBT-ASD-2** at 438 and 545 nm did not change with changing pH level from 3 to 11 (**Fig. S3a**

and **S3b**). This finding further indicated that **HBT-ASD-1** and **HBT-ASD-2** showed a spectral response that needs to be firstly activated by **NAS-DCE**. Furthermore, **HBT-ASD-1** and **HBT-ASD-2** presented strong photostability (**Fig. S4** and **S5**) and a negligible cytotoxicity (**Fig.S6**). The **HBT-ASD-1** and **HBT-ASD-2** possessed potential ability for sorting of cells and real-time monitoring of enzymatic activity.

8. HPLC monitors the recognition products of HBT-ASD-2

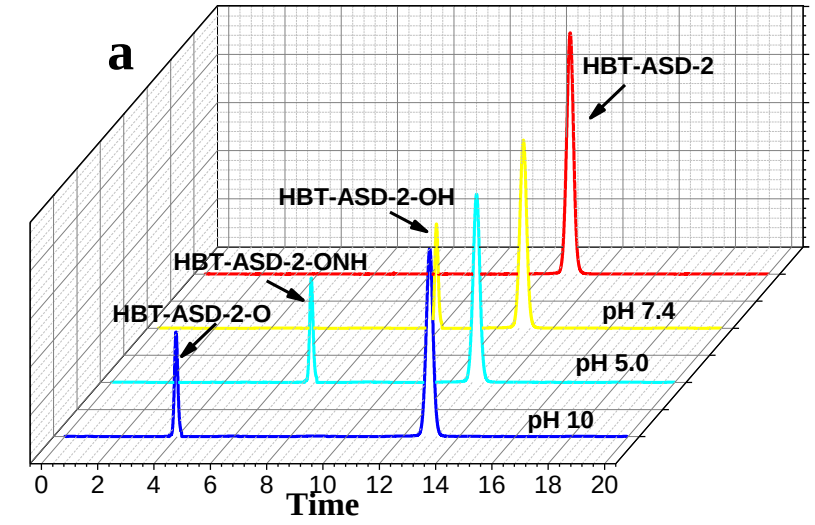

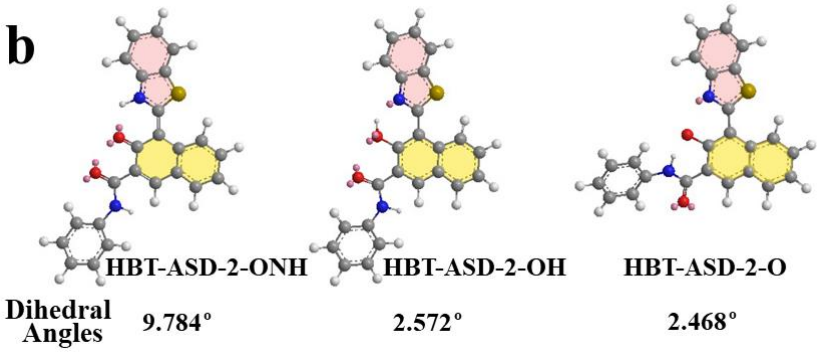

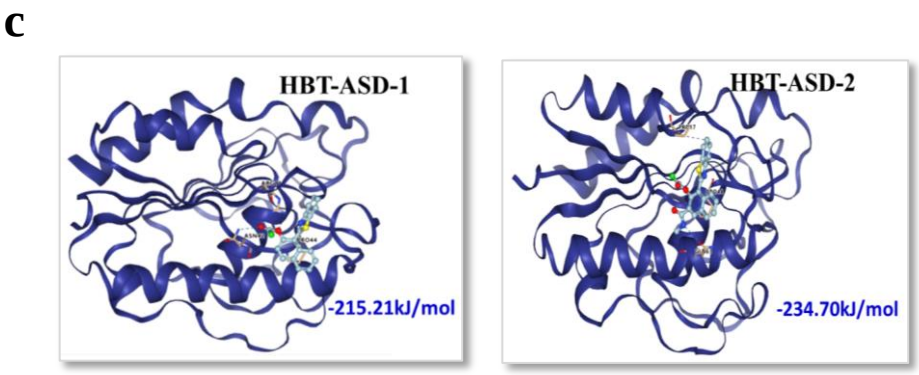

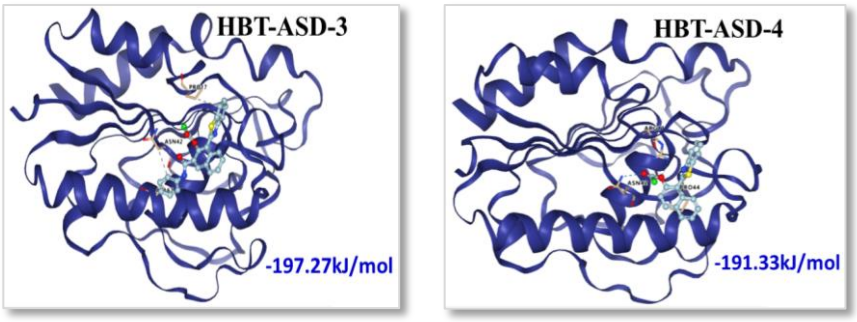

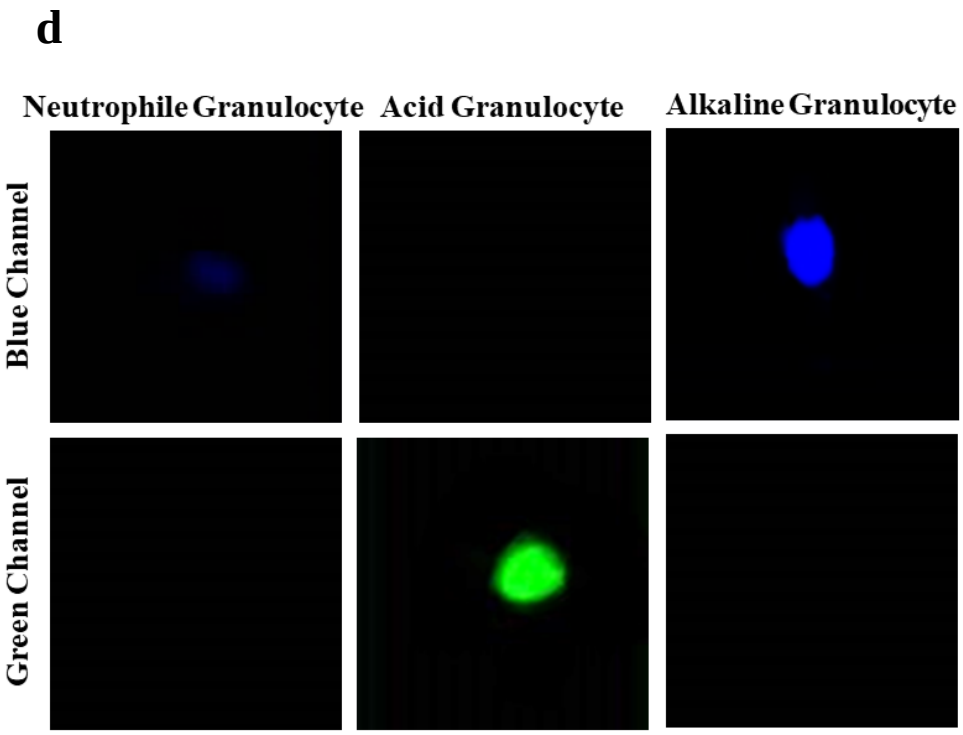

Figure S7. (a) HPLC monitor the recognition products of **HBT-ASD-2** (10 μM) with **NAS-DCE** (20 unit) in pH 7.4, pH 5.0 and pH 10. (b) the configuration optimization of **HBT-ASD-2-ONH**, **HBT-ASD-2-OH** and **HBT-ASD-2-O** by Gaussian 16 and their dihedral angles. The dihedral angles were between pink and yellow rigid plane. (c) The molecular docking of **HBT-ASDs** for **NAS-DCE** (PDB CODE:1bs9). (d) Imaging at the single cell level. HBT-O-2 (5.0 μM) for different granulocyte (acid, neutrophil and alkaline granulocytes). Fluorescence collection wavelength for blue channel at 410-460nm and green channel at 500-550 nm; excited at 405 nm.

To further elucidate the response mechanism of **HBT-ASD-2** for **NAS-DCE**, that is, the occurrence of the ESIPT process, the recognition products of **HBT-ASD-2** were monitored by HPLC (**Fig. S7a**). To verify the suitable substrate for **NAS-DCE**, the Gaussian 16 and molecular docking as the classical theoretical derivation methods were used to obtain the optimal configuration and the boding mode.

9. The content of different leukocyte in the pathological samples

Table S2. The content of different leukocyte in the pathological samples

	Neutrophil Granulocyte		Alkaline Granulocyte		Acid Granulocyte		Lymphocyte and Monocyte	
	Experimental Method	Control Method	Experimental Method	Control Method	Experimental Method	Control Method	Experimental Method	Control Method
Normal Mice	53.52%	53.06%	0.85%	0.91%	4.03%	4.15%	41.60%	41.88%
Plumbism Mice (Sample I)	57.65%	57.22%	0.77%	0.69%	3.99%	4.01%	37.59%	38.08%
Acidosis Mice (Sample II)	61.32%	61.54%	0.69%	0.72%	3.87%	3.95%	34.12%	33.79%

References

S1. Zhou, L.C., Zhao, G.J., Liu, J.F., Han, K.L., Wu, Y.K., Peng, X.J., Sun, M.T. J. *Photochem. Photobiol. A: Chem*. **2007**, 187:305.

S2. Dreizler, M.R., Gross, U., Density, E.K., **1990**. Functional Theory. Springer Verlag, Heidelberg.

Attached Spectra.

^{1}H NMR of HBT-COOH

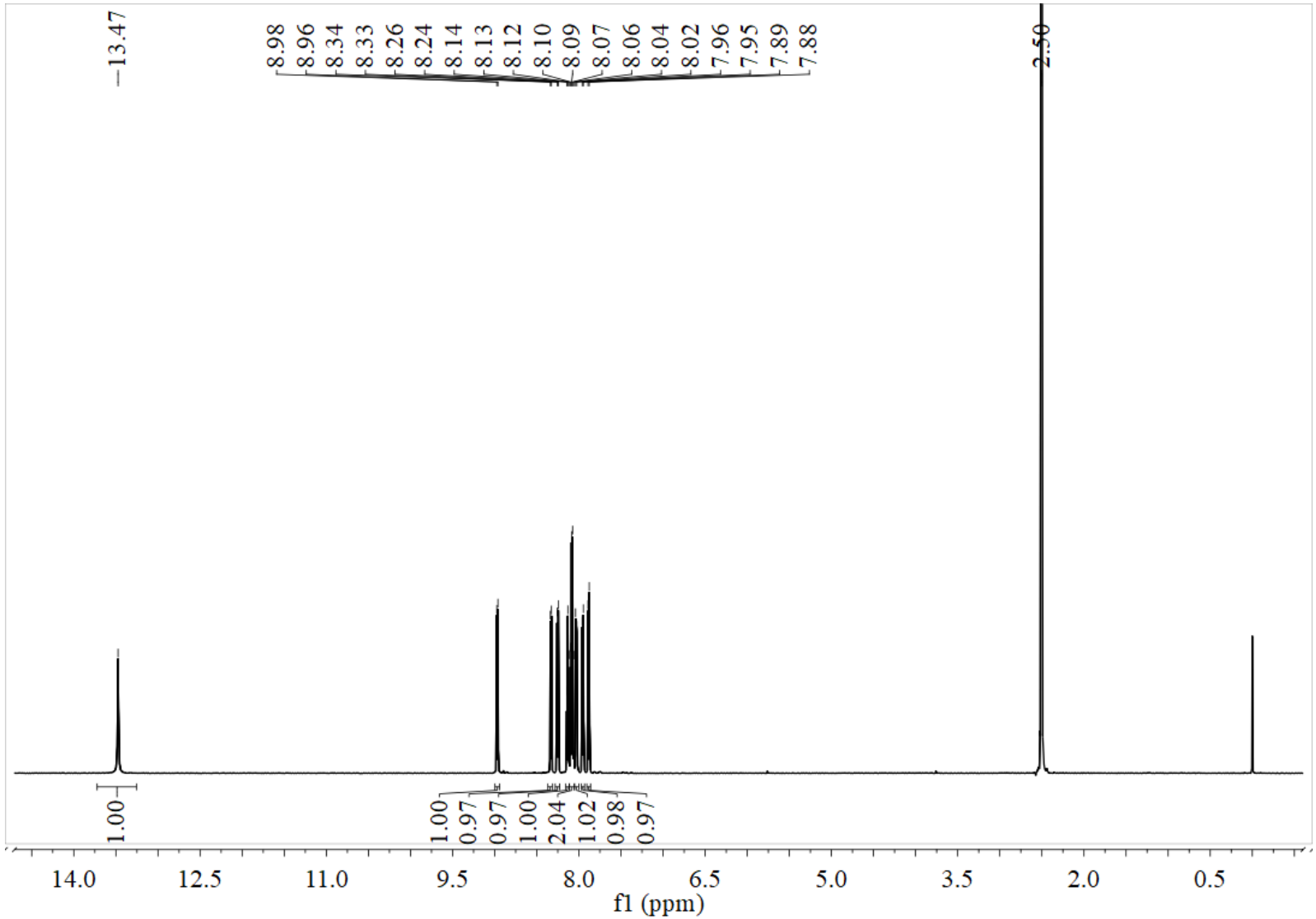

^{13}C NMR of HBT-COOH

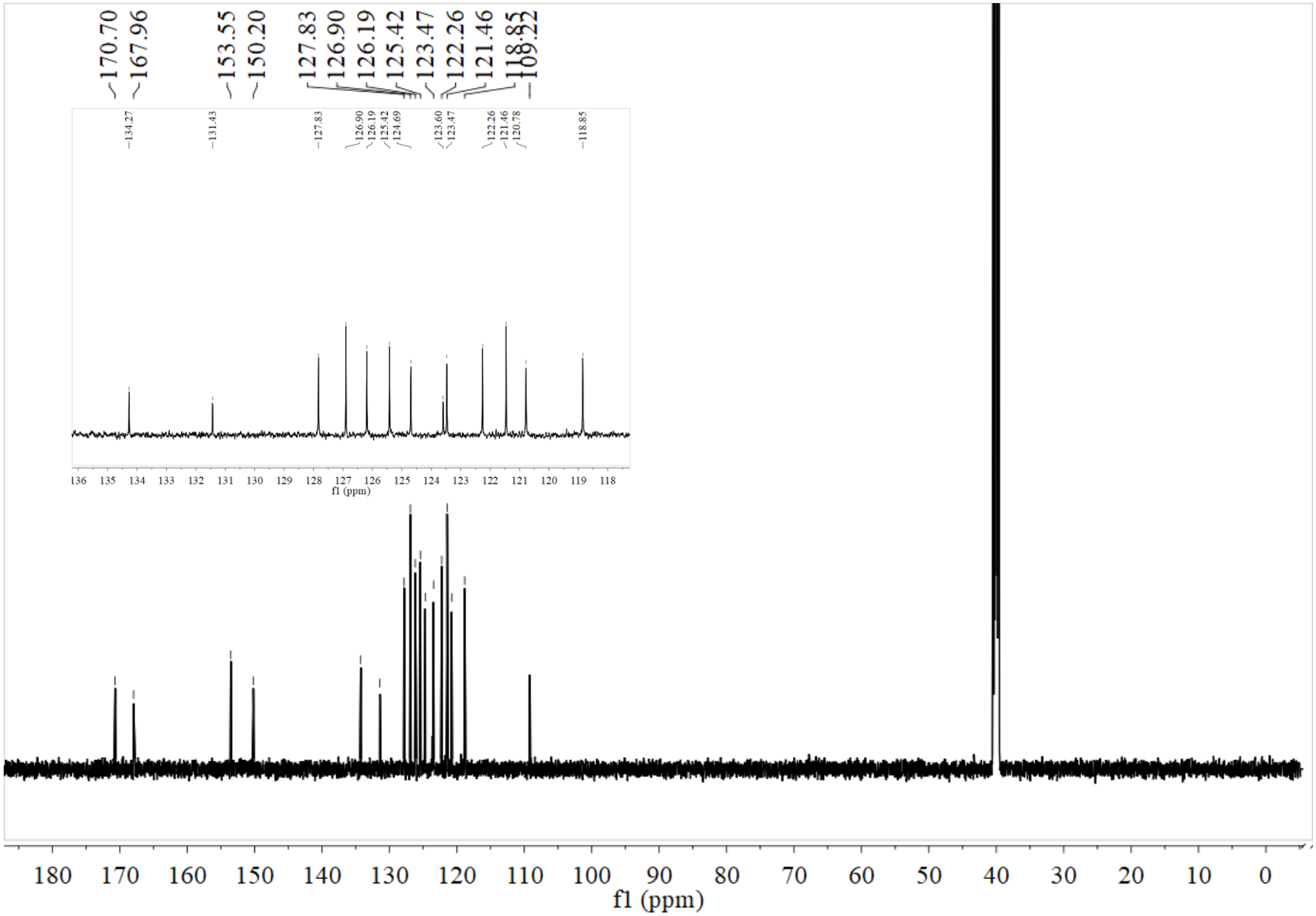

^{1}H NMR of HBT-O-1

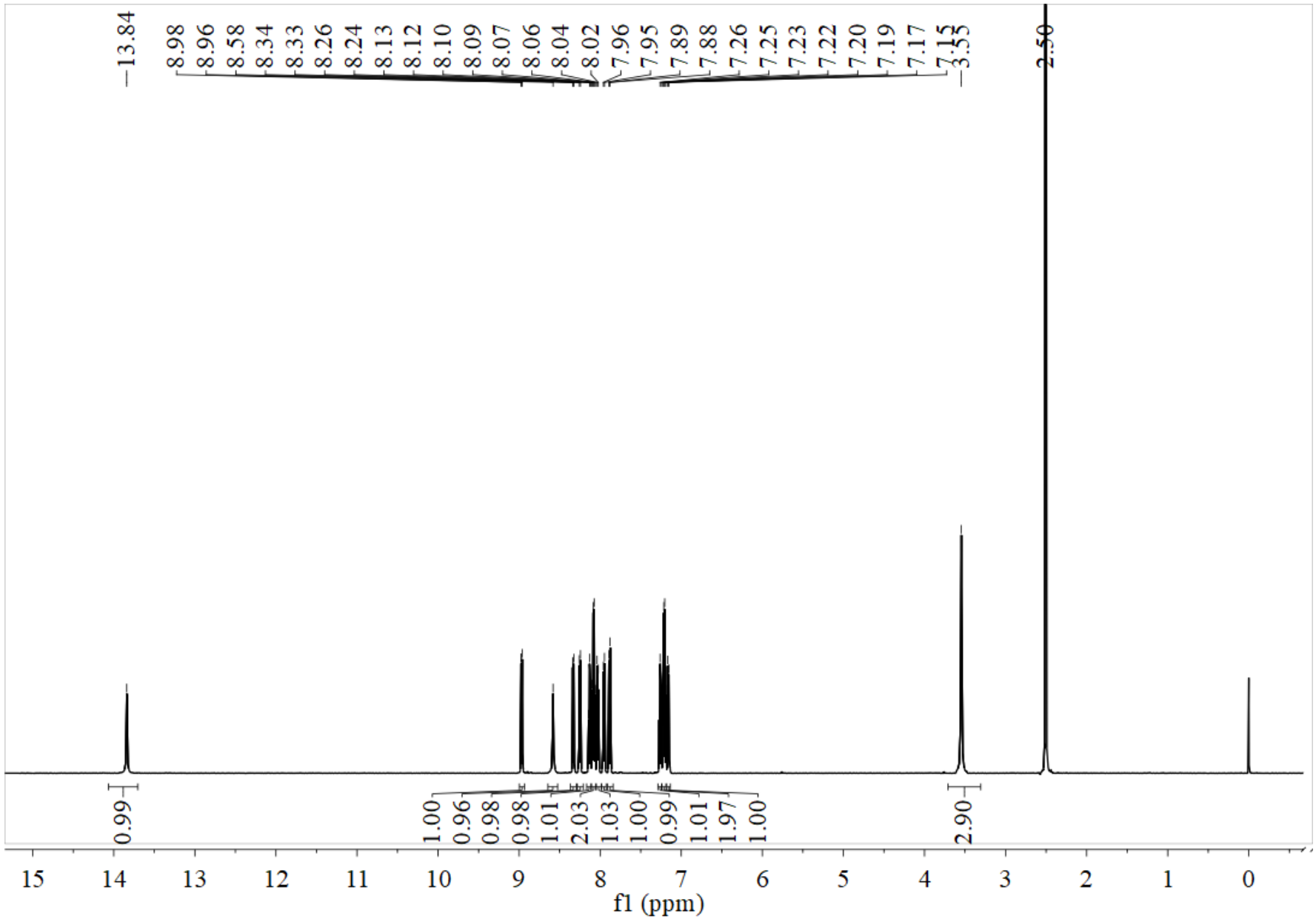

^{13}C NMR of HBT-O-1

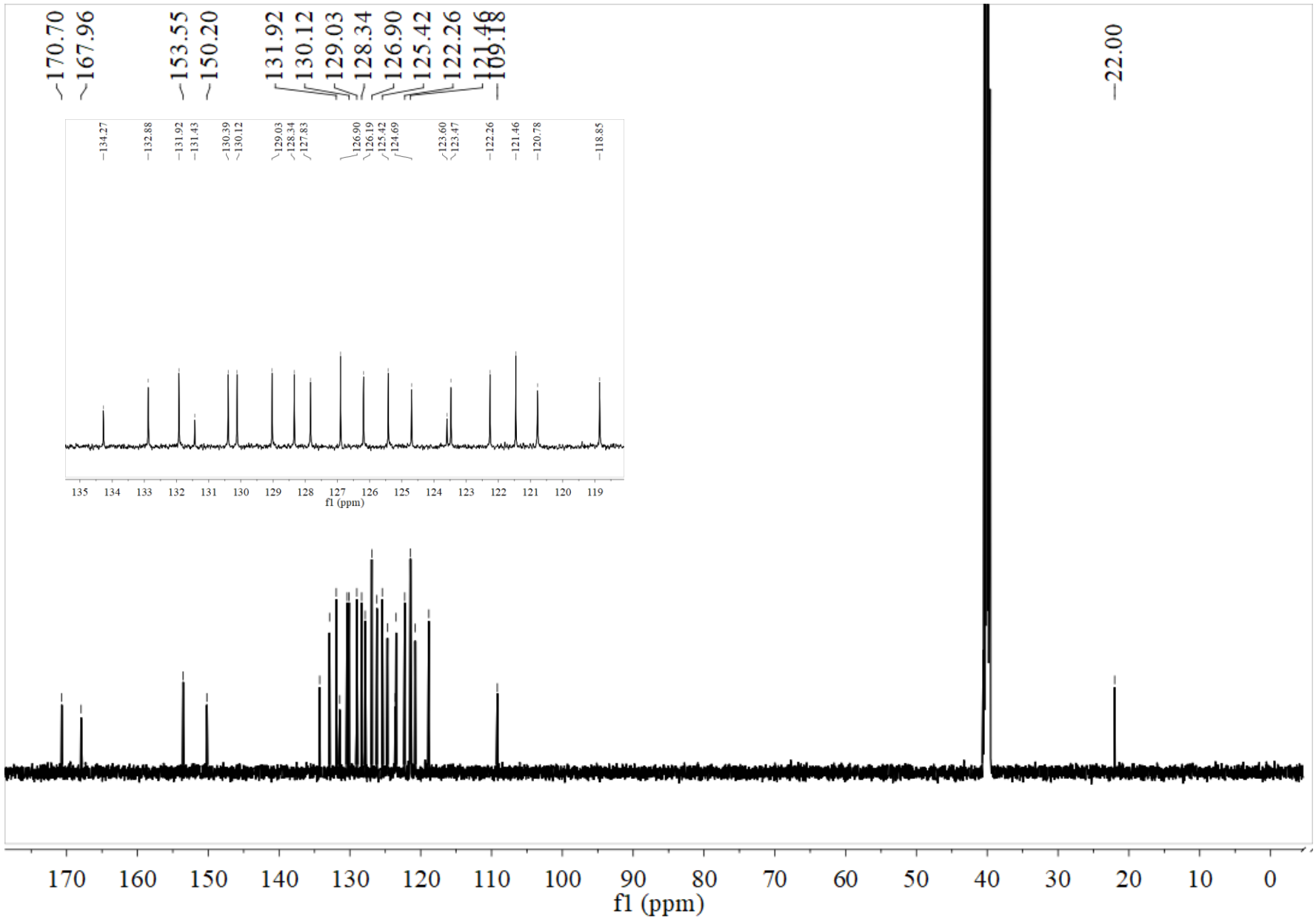

^{1}H NMR of HBT-O-2

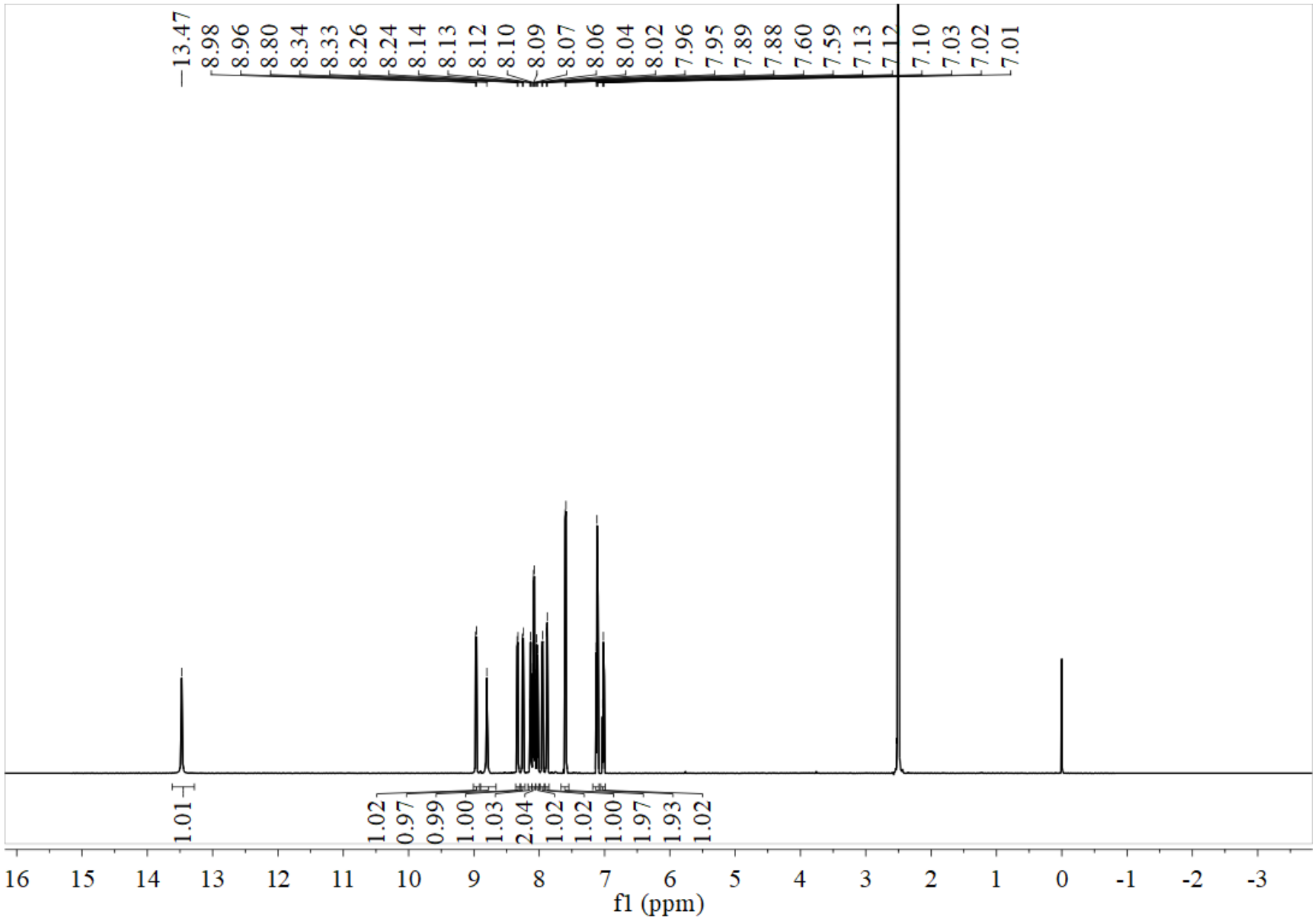

^{13}C NMR of HBT-O-2

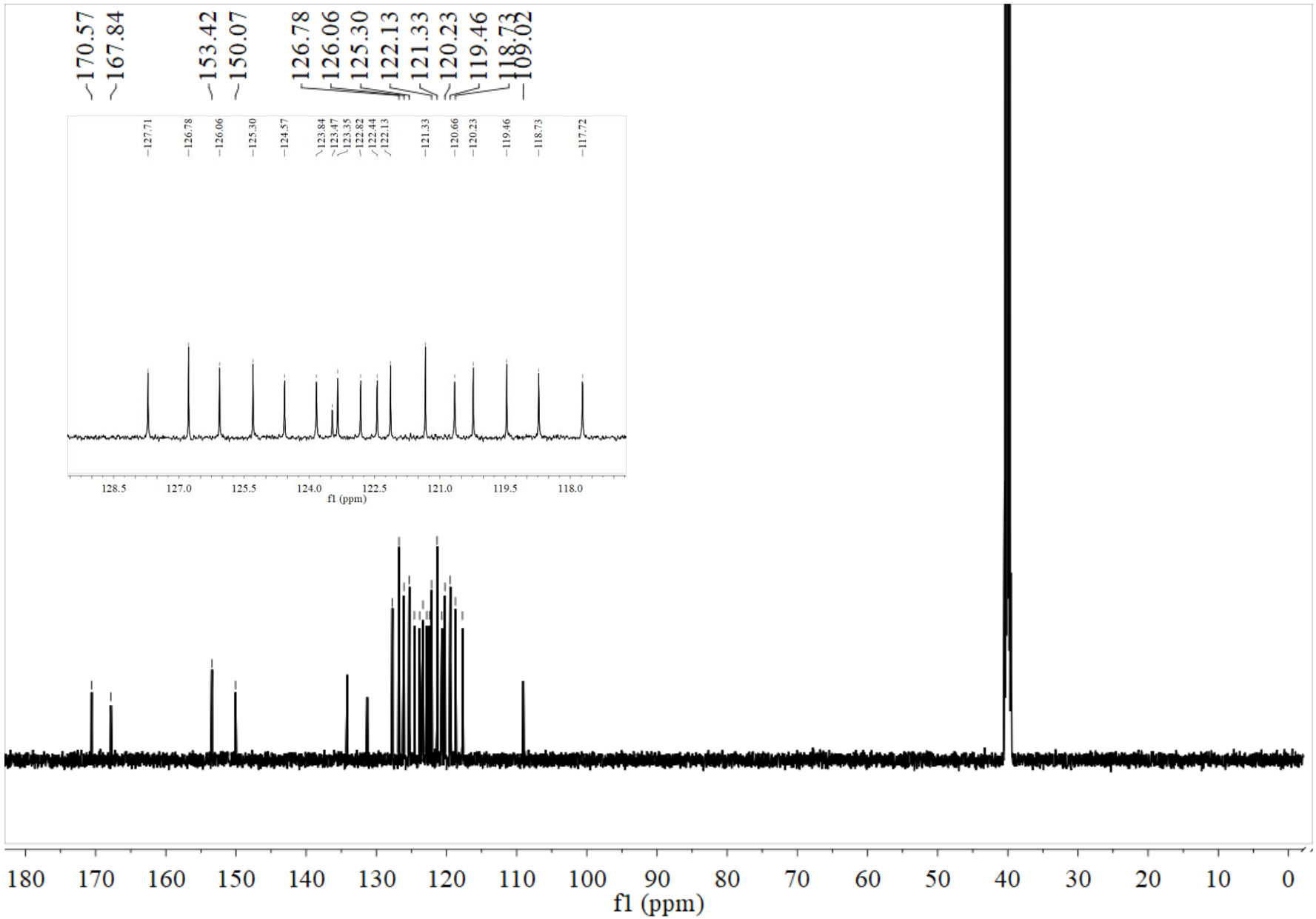

^{1}H NMR of HBT-O-3

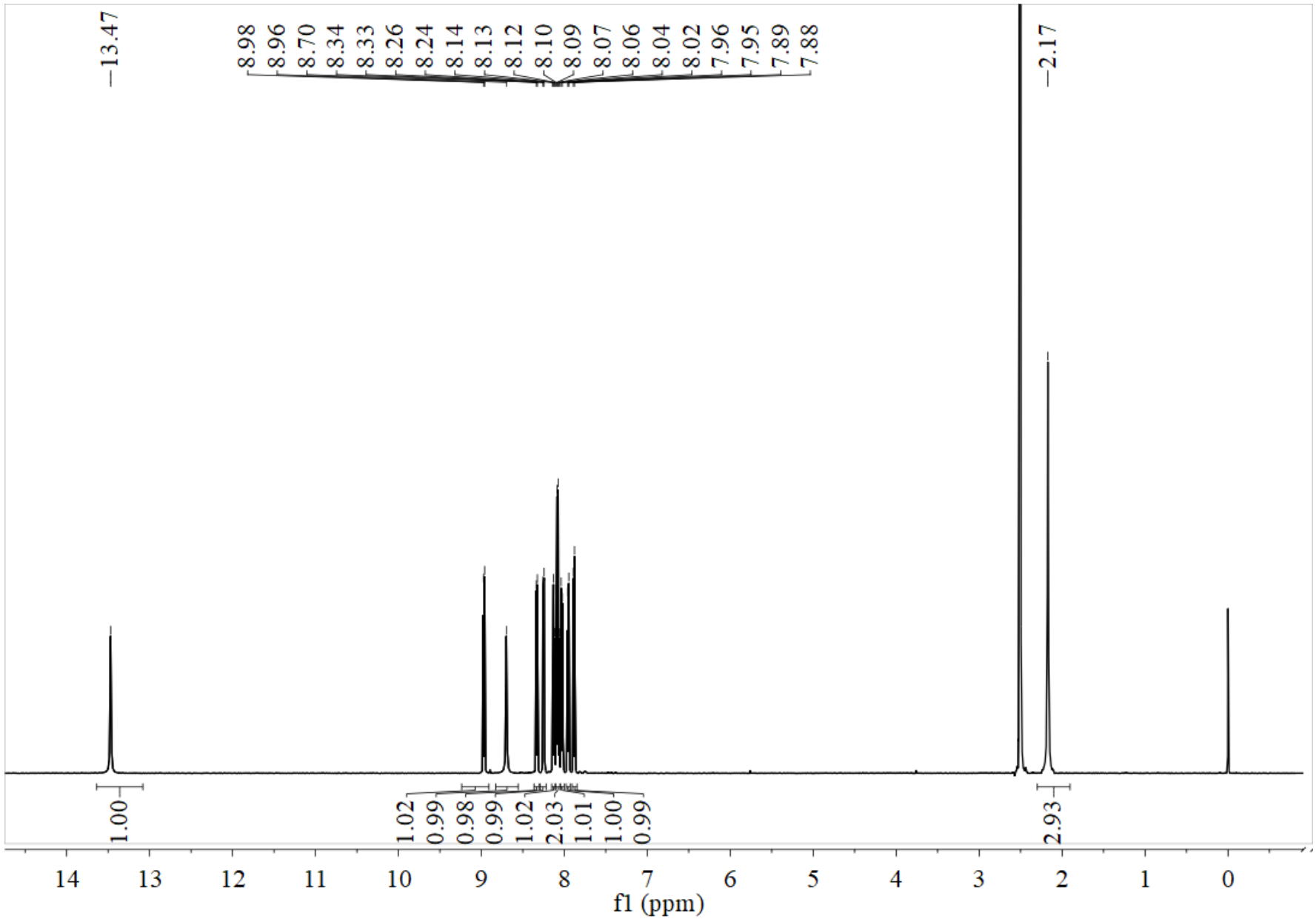

^{13}C NMR of HBT-O-3

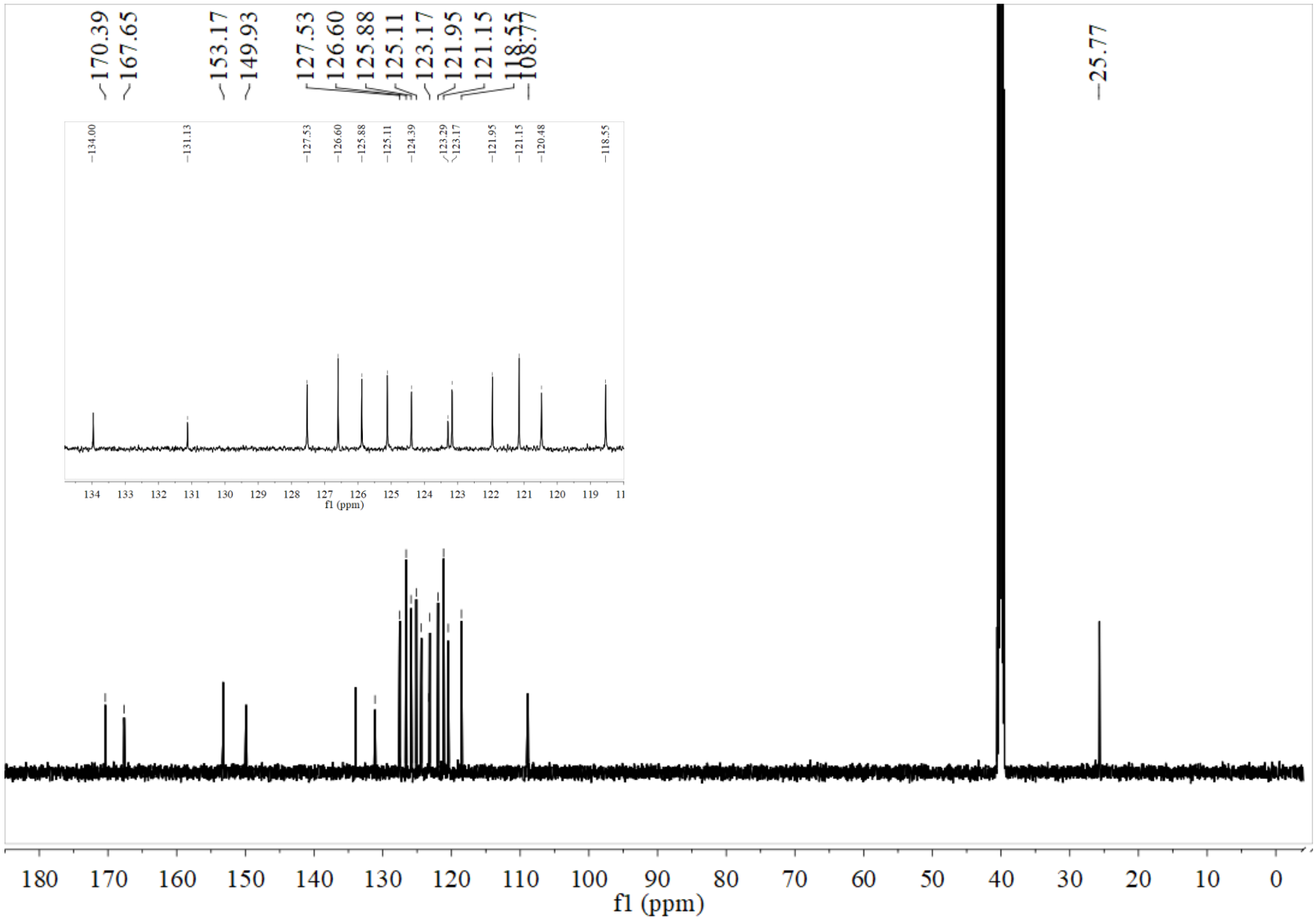

^{1}H NMR of HBT-O-4

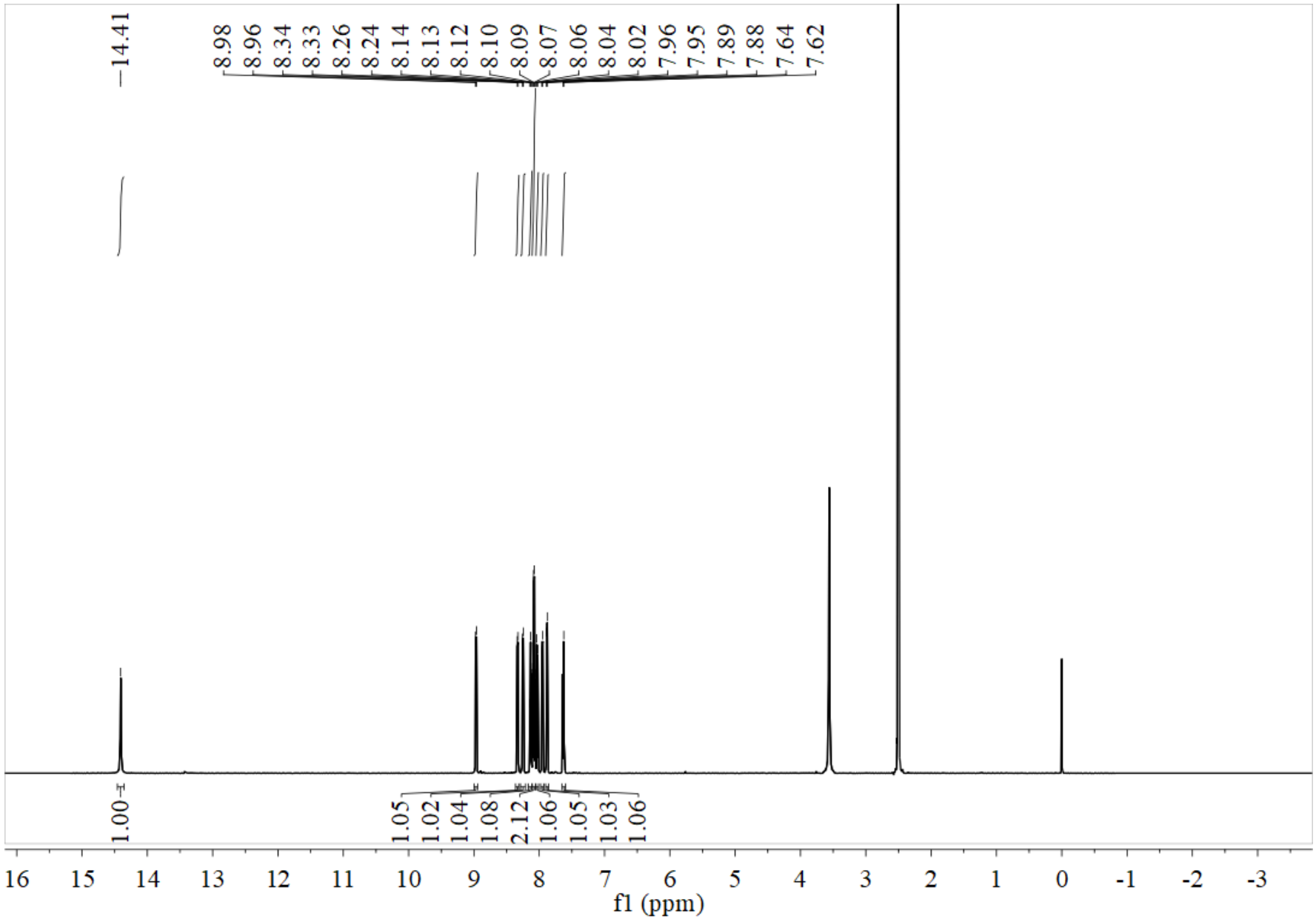

^{13}C NMR of HBT-O-4

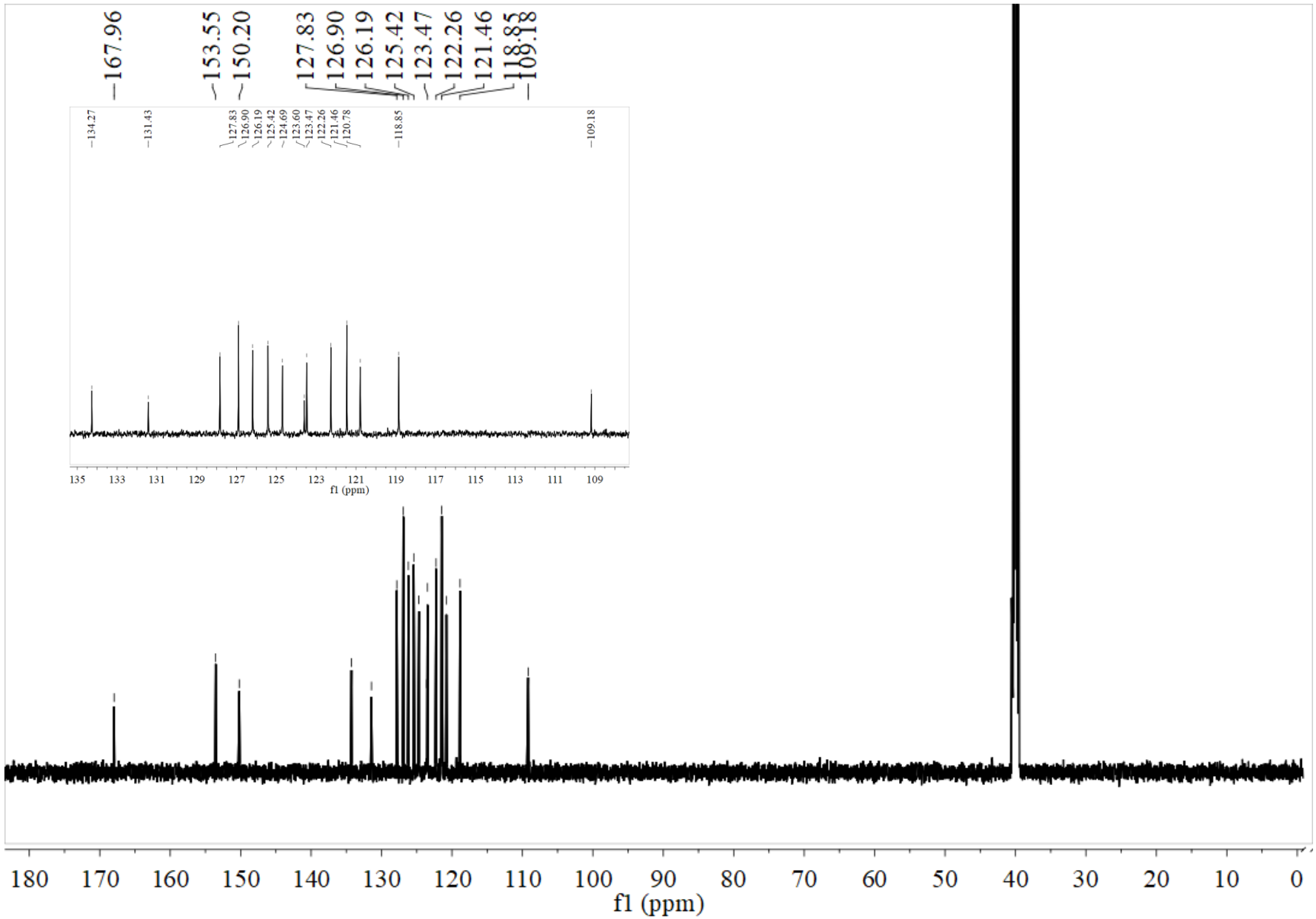

^{1}H NMR of HBT-ASD-1

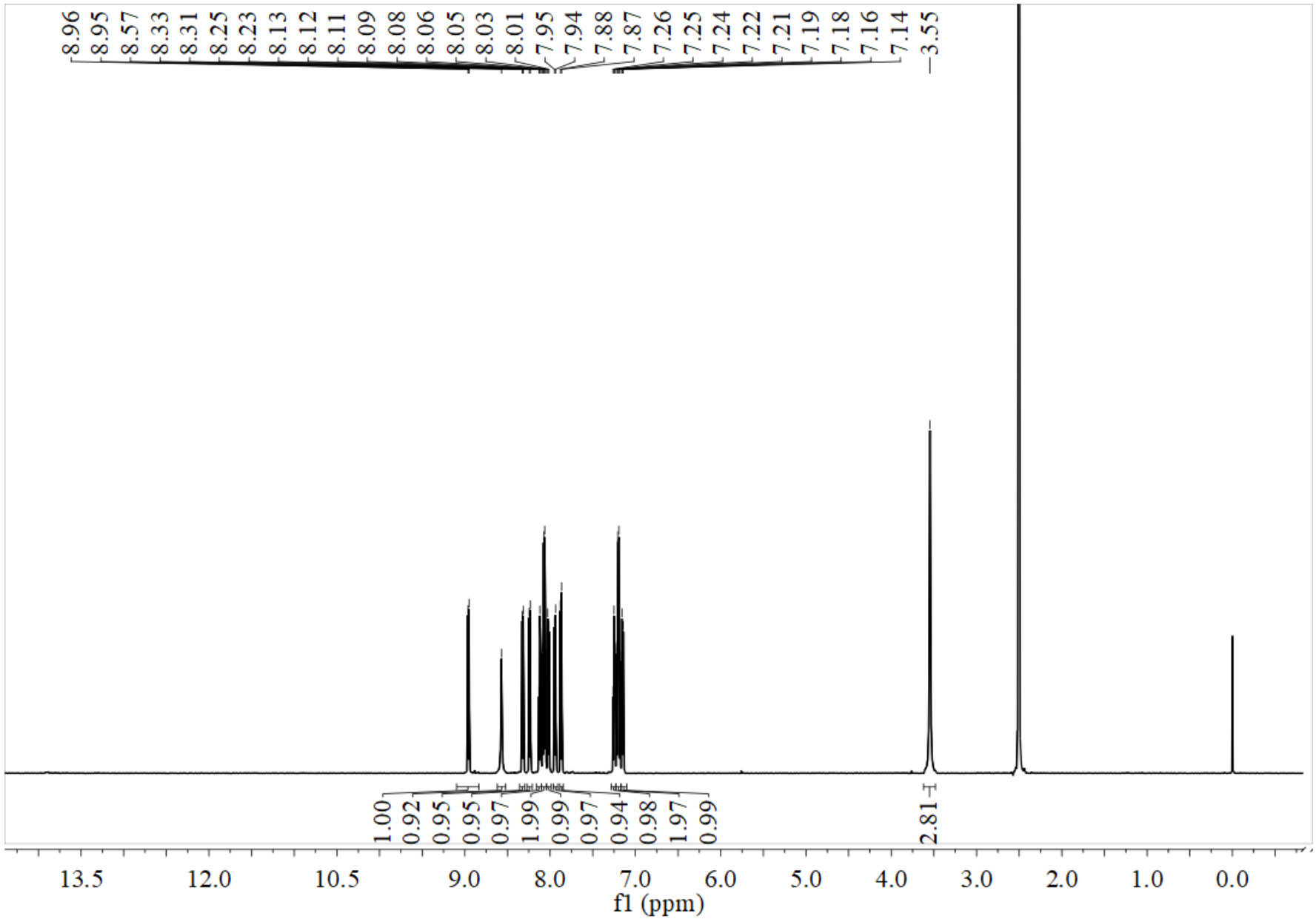

^{13}C NMR of HBT-ASD-1

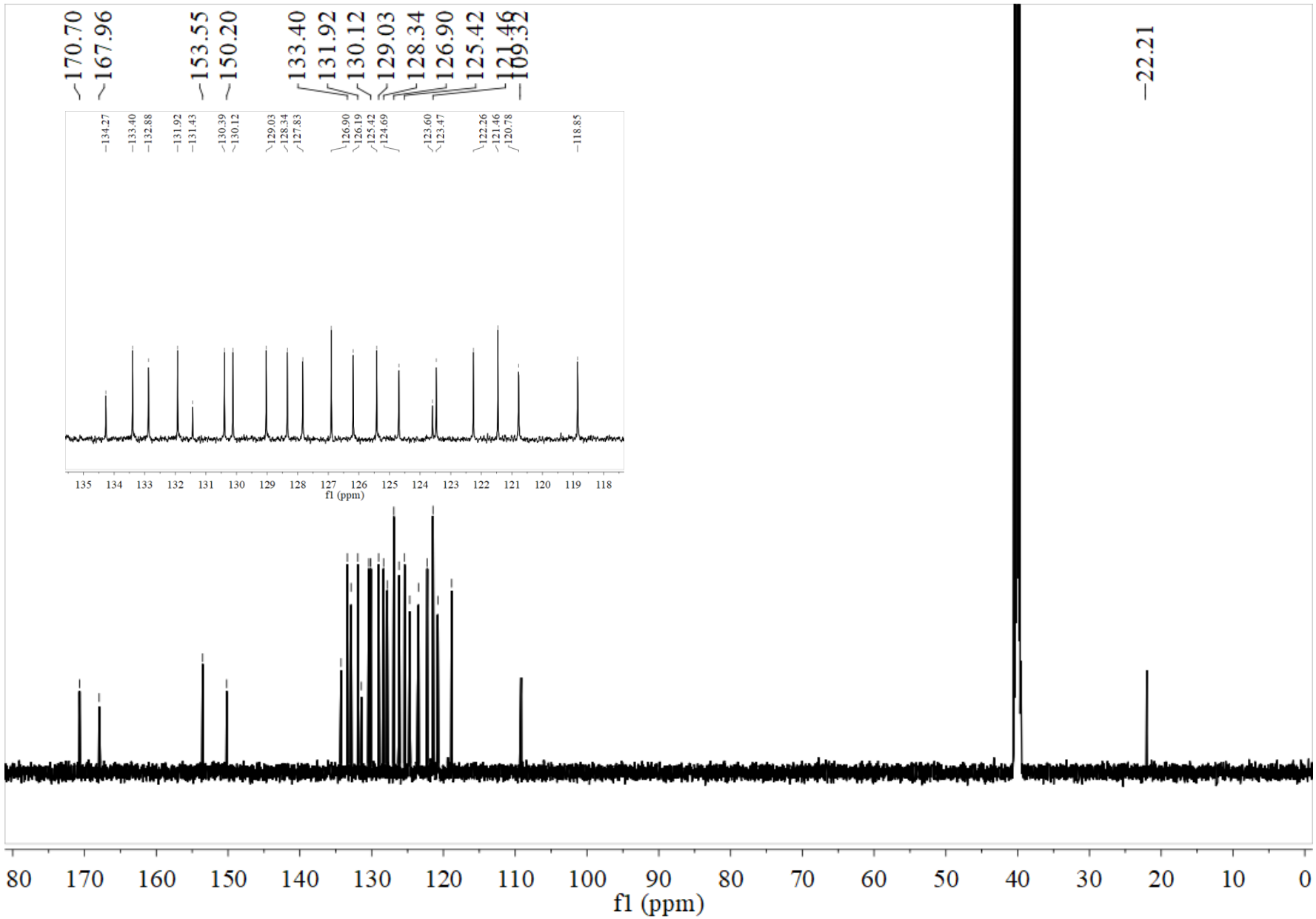

^{1}H NMR of HBT-ASD-2

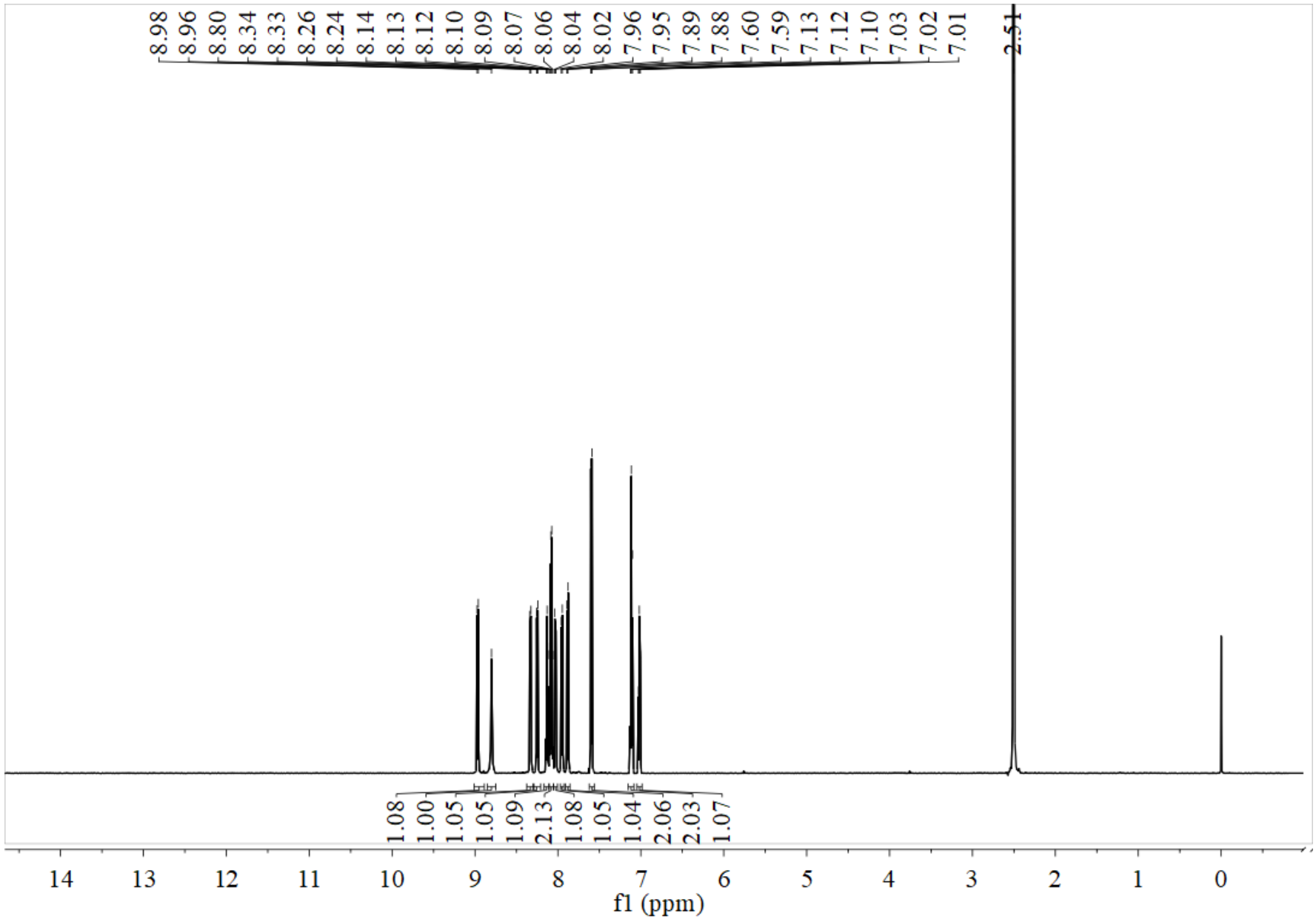

^{13}C NMR of HBT-ASD-2

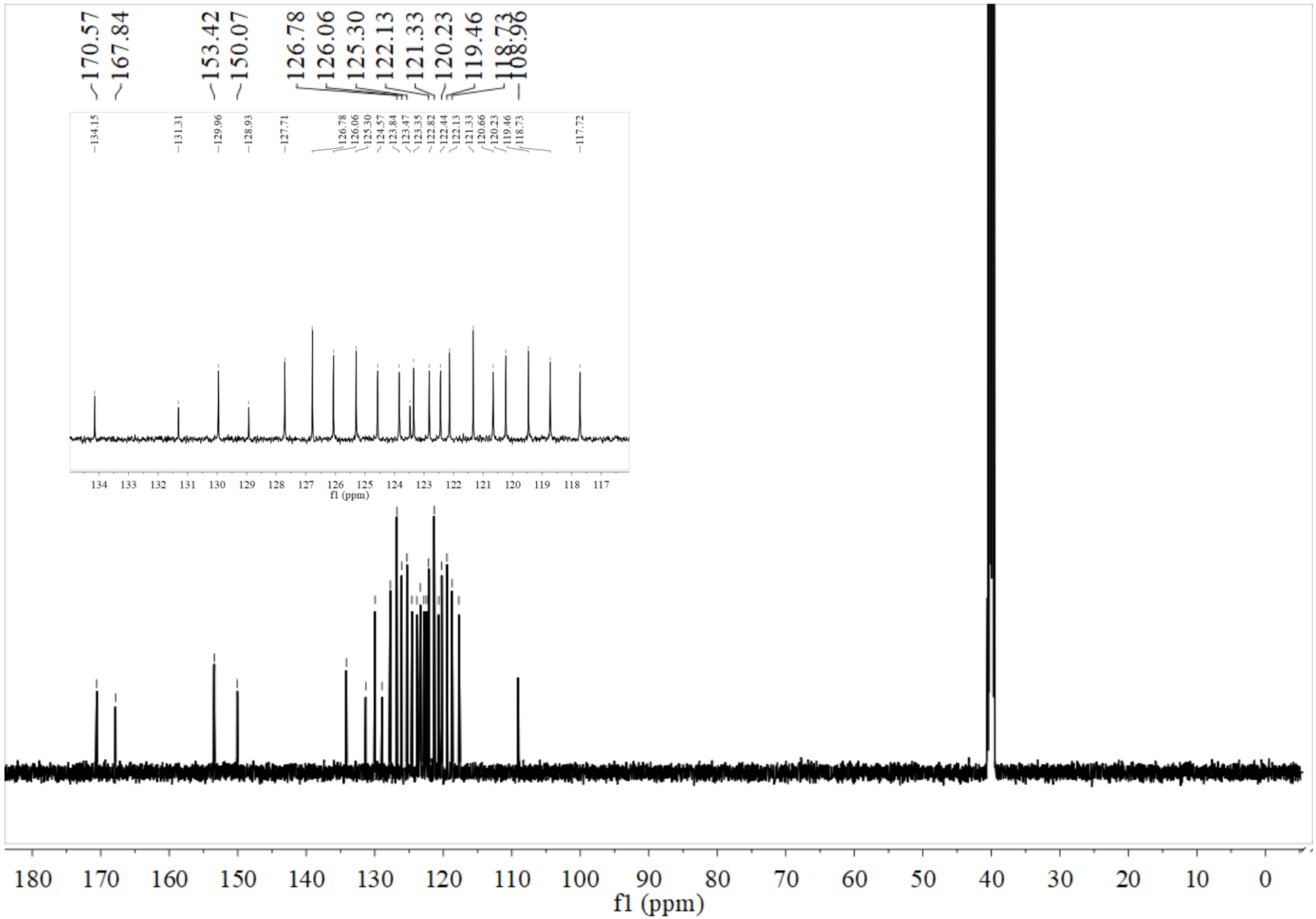

^{1}H NMR of HBT-ASD-3

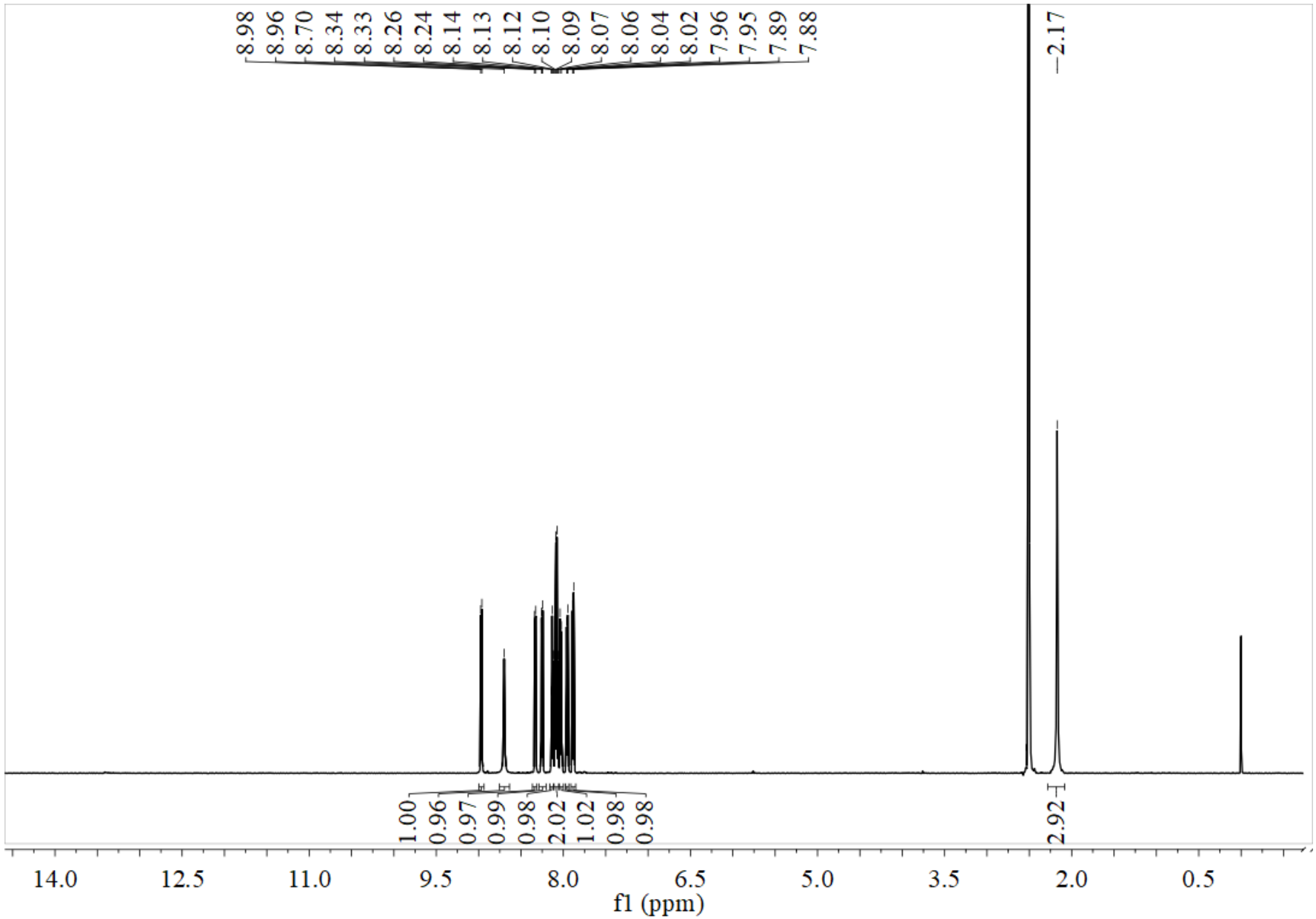

^{13}C NMR of HBT-ASD-3

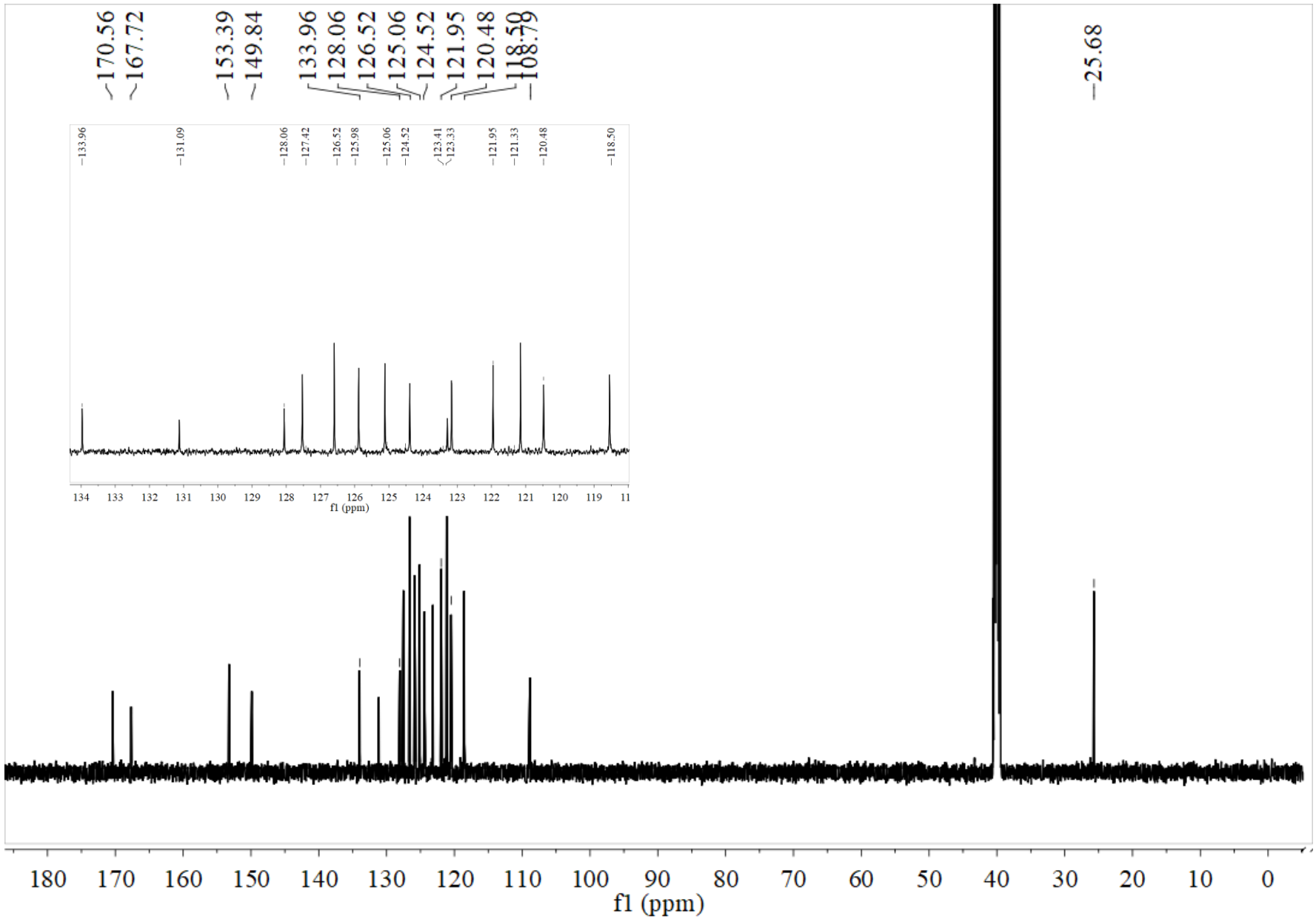

^{1}H NMR of HBT-ASD-4

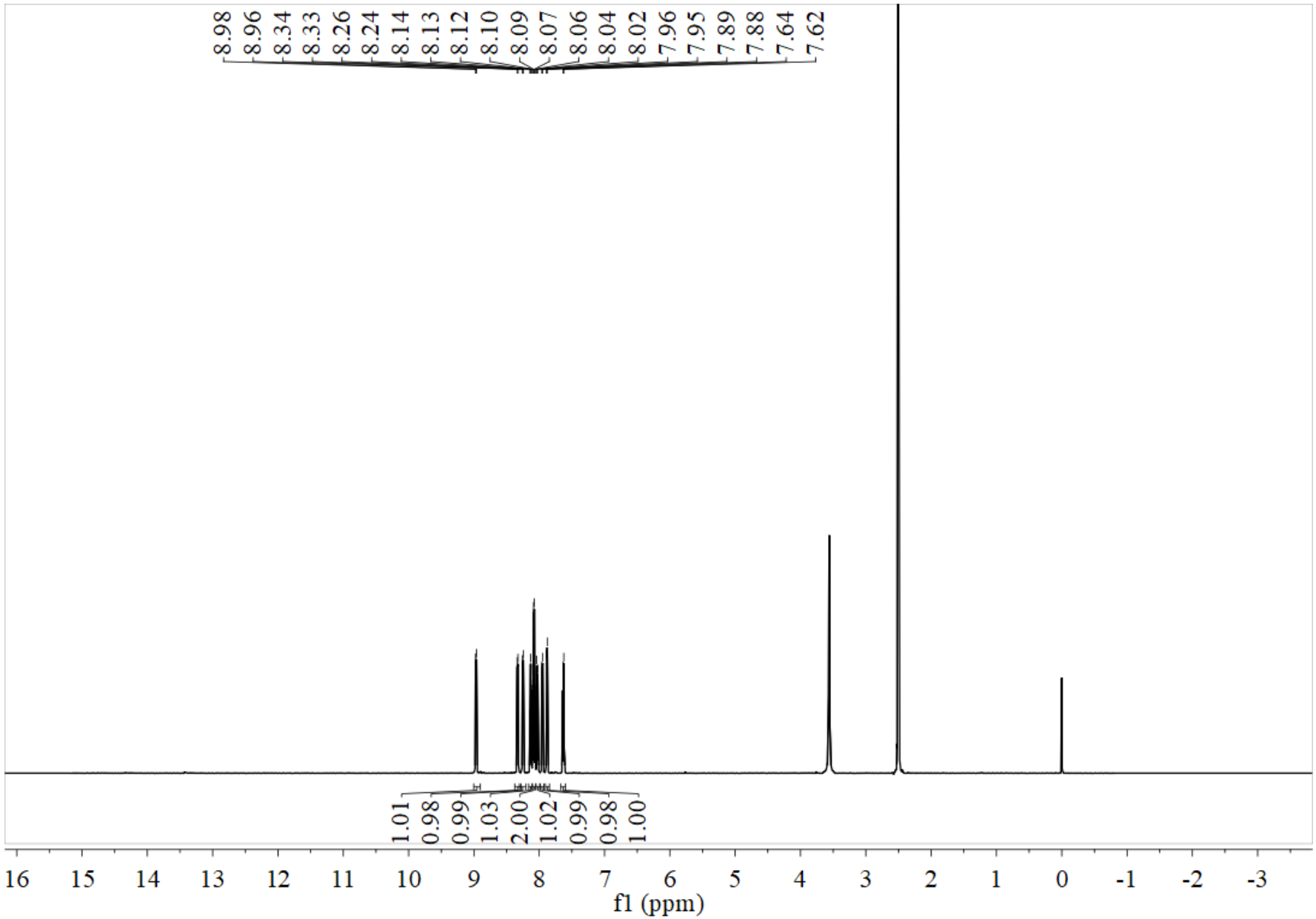

^{13}C NMR of HBT-ASD-4